A command-like descending neuron that coordinately activates backward and inhibits forward locomotion

Arnaldo Carreira-Rosario[1#], Aref Arzan Zarin[1#], Matthew Q. Clark[1#^], Laurina Manning[1], Richard Fetter[2], Albert Cardona[2], and Chris Q. Doe[1*]

[1]Institute of Neuroscience, Institute of Molecular Biology, Howard Hughes Medical Institute, University of Oregon, Eugene, OR 97403

[2]Janelia Research Campus, Howard Hughes Medical Institute, Ashburn, VA 20147

# These authors contributed equally

^ Current address: Division of Biology and Biological Engineering, California Institute of Technology, Pasadena, CA 91125

* Author for correspondence at cdoe@uoregon.edu

Key words: behavioral switching, backward locomotion, crawling, walking, sensorimotor, wave propagation, descending interneuron, aversion, neural circuit, Drosophila

Highlights

- MDN command-like descending neuron induces backward larval locomotion
- MDN neurons coordinately regulate antagonistic behaviors (forward/backward locomotion)
- MDN-motor circuit validated at structural (TEM) and functional (optogenetic) levels
- MDN neurons induce backward locomotion in both limbless larva and limbed adult

Abstract

Command-like descending neurons can induce many behaviors, such as backward locomotion, escape, feeding, courtship, egg-laying, or grooming. In most animals it remains unknown how neural circuits switch between these antagonistic behaviors: via top-down activation/inhibition of antagonistic circuits or via reciprocal inhibition between antagonistic circuits. Here we use genetic screens, intersectional genetics, circuit reconstruction by electron microscopy, and functional optogenetics to identify a bilateral pair of larval “mooncrawler descending neurons” (MDNs) with command-like ability to coordinately induce backward locomotion and block forward locomotion; the former by activating a backward-specific premotor neuron, and the latter by disynaptic inhibition of a forward-specific premotor neuron. In contrast, direct reciprocal inhibition between forward and backward circuits was not observed. Thus, MDNs coordinate a transition between antagonistic larval locomotor behaviors. Interestingly, larval MDNs persist into adulthood, where they can trigger backward walking. Thus, MDNs induce backward locomotion in both limbless and limbed animals.

Introduction

Animals typically execute one behavior to the exclusion of all other possible behaviors. For example, during locomotion, an animal can either move forward or backwards, but cannot do both simultaneously. The selection of a locomotor program to the exclusion of all others is necessary to prevent injury and escape predation. Despite the paramount importance of rapid transitions between antagonistic motor programs, the underlying circuitry is only beginning to be understood in *C. elegans* (Lindsay et al., 2011; Piggott et al., 2011; Roberts et al., 2016).

Command neurons can elicit specific behaviors, such as forward locomotion, backward locomotion, pausing, escape, flight, grooming, feeding, courtship, egg-laying or sleep (Bidaye et al., 2014; Bouvier et al., 2015; Hagglund et al., 2010; Hampel et al., 2015; Hedwig, 2000; Hückesfeld et al., 2015; Kallman et al., 2015; Liu and Fetcho, 1999; Ohyama et al., 2015; Pearson et al., 1985; Sen et al., 2017; Tanouye and Wyman, 1980; von Philipsborn et al., 2011; Weber et al., 2015; Wu et al., 2015). However, much less is known about how antagonistic motor programs are suppressed during command neuron induced behavior. On one hand, there could be a high degree of reciprocal inhibition between neurons in antagonistic circuits; on the other hand, the command neurons that activate one behavior may also suppress antagonistic behaviors (in which case there could be minimal reciprocal inhibition). Here we use the *Drosophila* larva to characterize the neural circuits coordinately regulating two antagonistic behaviors: forward versus backward locomotion.

Drosophila larva have many distinct behaviors (Vogelstein et al., 2014), but forward locomotion is the default locomotor behavior (Berni et al., 2012) and consists of coordinated posterior-to-anterior waves of somatic body wall muscle contractions driven by corresponding waves of motor neuron activity within the segmented ventral nerve cord (VNC) (Clark et al., 2018; Heckscher et al., 2012; Hughes and Thomas, 2007; Pulver et al., 2015). There are ~35 motor neurons per bilateral hemisegment, innervating 30 body wall muscles (Landgraf and Thor, 2006), about 250 interneurons per hemisegment (Rickert et al., 2011), and an unknown number of ascending and descending neurons traversing each segment of the VNC. The circuits for motor wave propagation (Fushiki et al., 2016), the coordination of muscle groups within each segment (Zwart et al., 2016), and the bilateral adjustment of muscle contraction amplitude (Heckscher et al., 2015) have been recently investigated; however, much less is known about the circuits promoting backward locomotion, or the switching from forward to backward locomotion.

Larvae initiate backward locomotion upon encountering a barrier or experiencing mild noxious stimulation to the anterior body (Kernan et al., 1994; Robertson et al., 2013; Takagi et al., 2017; Titlow et al., 2014; Tracey et al., 2003). Backwards locomotion consists of anterior-to-posterior waves of motor neuron and muscle activity (Heckscher et al., 2012; Pulver et al., 2015). A segmentally-reiterated VNC neuron that triggers backward locomotion has been identified (Takagi et al., 2017), but high-order command neurons for backward locomotion and the circuit for

executing backwards wave propagation while simultaneously suppressing forward waves remain unknown.

Here, we identify a bilateral pair of *Drosophila* brain descending neurons that coordinately activate backward locomotion and suppress forward locomotion, and identify the downstream pre-motor circuitry effecting the switch. Surprisingly, immortalization of CsChrimson (Chrimson) expression in these larval command-like neurons reveals that they survive metamorphosis, have the exact morphology of previously described adult "moonwalker" neurons (Bidaye et al., 2014), and can induce backward walking in the adult. By analogy to the adult naming scheme, we refer to these larval brain neurons as "mooncrawler descending neurons" (MDNs). We reconstruct the larval MDNs in an electron microscopy volume comprising the whole central nervous system (Ohyama et al., 2015), in which we also map its postsynaptic neuron partners. We identify the circuit motifs by which MDNs induce backward locomotion while simultaneously suppressing forward locomotion. The MDNs project their axons along the length of the nerve cord, where they directly activate an excitatory cholinergic pre-motor neuron (A18b) that is specifically active during backward waves. In parallel, the MDNs synapse onto a GABAergic inhibitory neuron (Pair1) that directly inhibits cholinergic pre-motor neurons (A27h) active specifically during forward locomotion (Fushiki et al., 2016); optogenetic experiments showed that MDNs activate Pair1 neurons, which then inhibit A27h and block forward locomotion. The circuit structure therefore suggests that two behaviors such as forward and backward peristaltic locomotion can maintain mutually exclusive activity due to top-down excitation/inhibition, rather than reciprocal inhibition. We conclude that the MDNs promote backward locomotion at all stages of the *Drosophila* life cycle: from the limbless crawling maggot to the limbed walking adult.

Results

Identification of brain neurons sufficient and necessary for larval backward locomotion

We previously showed that activating neurons labeled by the Janelia R53F07-Gal4 line could induce backward larval locomotion, but this line has broad expression in the brain, subesophageal zone (SEZ), and both motor neurons and interneurons of the VNC (Clark et al., 2016). To identify the neurons within this population that can induce backward locomotion, we used intersectional genetics (Dolan et al., 2017; Luan et al., 2006) to find lines labeling small subsets of the original population. We identified three lines called Split1, Split2, and Split3 labeling different subsets of the original pattern; the only neurons present in all three Split lines are a bilateral pair of neurons with cell bodies located in the ventral, anterior, medial brain with descending processes to A3-A5 in the VNC (**Figure 1A-C**, arrowheads).

All three Split lines could induce backward locomotion following Chrimson expression and activation (**Figure 1D**, Movie 1). Neuronal activation immediately switched locomotion from forward to backward (**Figure 1E,F**), without a significant change in the number of peristaltic

waves per second (Split1, 0.48; Split2, 0.50; Split3, 0.65 before activation; Split1, 0.48; Split2, 0.56; Split3, 0.56 after activation). Conversely, using Split2 or Split3 to express the light-inducible neuronal silencer GtACR1 (Mohammad et al., 2017) significantly reduced backward locomotion induced by a noxious head poke (**Figure 1G,H**). It is likely that these activation and silencing phenotypes arise from the pair of ventral, anterior, medial brain descending neurons common to all three lines, although it is possible that there are different neurons in each Split line that can induce backward locomotion. We distinguish between these alternatives in the next section.

A single pair of brain neurons can induce a switch from forward to backward locomotion

To determine whether Chrimson expression in just one or two of the ventral, anterior, medial brain neurons is sufficient to induce backwards locomotion, we stochastically expressed Chrimson:Venus within the Split2 pattern via the "FLP-out" method (**Figure 2A**). We screened populations of larvae for Chrimson-induced backward locomotion (obtaining 1-2 larvae per 100 screened), and stained the CNS to identify the Chrimson:Venus^{+} neurons that were sufficient to induce backward locomotion. All larvae with a backward locomotion phenotype (n=10) expressed Chrimson:Venus in one or both neurons from the anterior, medial pair that had descending projections to A3-A5 (three examples shown in **Figure 2B-D**). Conversely, all larvae that lacked Chrimson-induced backward locomotion (n=20) never showed Chrimson:Venus expression in the ventral, anterior, medial descending neurons (data not shown). Based on similarity to the "moonwalker" neuron adult backward walking phenotype (Bidaye et al., 2014), we name this bilateral pair of neurons the "mooncrawler" descending neurons (MDNa and MDNb), subsequently called MDNs. The MDNs are likely to be excitatory, as they are cholinergic (**Figure 2E**). We conclude that activation of as few as two of the four MDNs (either both in the same brain lobe or one in each brain lobe) is sufficient to induce a behavioral switch from forward to backward locomotion.

If forced activation of MDNs can induce backward locomotion, perhaps the MDNs are normally active specifically during backward locomotion. To test this hypothesis, we used CaMPARI to monitor MDN activity during forward versus backward locomotion within the intact crawling larva. CaMPARI undergoes an irreversible green-to-red conversion upon coincident exposure to elevated Calcium (i.e. neuronal activity) and 405nm illumination (Fosque et al., 2015). We used Split2 to express CaMPARI in MDNs and exposed crawling larvae to 405nm illumination for 30 sec during either backward or forward locomotion. We detected little or no activity-induced red fluorescence during forward locomotion, but significant red fluorescence during backward locomotion (**Figure 2F**). Note that not all backward crawling larvae activate MDN; we return to this point below. We conclude that MDNs are active during backward but not forward locomotion.

158 **Identification of MDNs in a serial section TEM reconstruction of the larval CNS**

159 To understand how MDNs induce backward locomotion, we next identified the MDN
160 synaptic partners. To do this, we identified the MDNs in an existing serial section TEM
161 reconstruction of the newly hatched larva (Ohyama et al., 2015). Our first step was to
162 determine the precise morphology of both MDN neurons. We generated individually labeled
163 neurons within the Split2 pattern using MultiColor FlpOut (MCFO) (Nern et al., 2015). These
164 single neurons serve as the "ground truth" for matching morphological features of individual
165 neurons by light and electron microscopy (Heckscher et al., 2015; Schneider-Mizell et al.,
166 2016). We identified single MDNs in Split2 MCFO preparations based on morphological
167 similarity to the behavior flip-out neurons described in **Figure 2**. Diagnostic features shared by
168 both MDNs in the pair include ventral, anterior, medial somata, distinctive ipsilateral and
169 contralateral arbors, a contralateral projection in the posterior commissure, and descending
170 neurons terminating in segments A3-A5 of the VNC (**Figure 3A-E**). Both MDNs have
171 descending axons that run slightly lateral to the dorsal medial FasII^{+} bundle (Landgraf et al.,
172 2003)(**Figure 3F**). Each neuron in the pair share all of these features, as well as common inputs
173 and outputs (see below), but the two MDNs can be distinguished from each other by their
174 ipsilateral arbor, which is either linear (**Figure 3C**, arrow) or bushy (**Figure 3D**, arrowhead). We
175 next searched for the MDNs in the TEM volume using CATMAID (Schneider-Mizell et al., 2016).
176 We found two pair of neurons that showed an excellent morphological match to the MDNs in
177 every distinctive feature (**Figure 3A'-D'**); we annotate them as MDNa and MDNb in the TEM
178 volume. Hereafter we call these neurons simply MDNs due to their similarity in morphology and
179 connectivity (see next section). Importantly, none of the 50 neurons with cell bodies nearest to
180 the MDNs have a similar morphology (data not shown). Thus, we can be certain that the MDNs
181 in the TEM reconstruction are identical to the MDNs visualized by our Split-gal4 lines. This is
182 also confirmed by functional optogenetics (see below). We conclude that the MDNs can be
183 uniquely identified by light microscopy and by TEM. Identification of the MDNs in the TEM
184 volume is a prerequisite for identifying their pre- and post-synaptic partners (next section).
185
186 **The MDN circuit: three pathways to distinct premotor neurons**
187 Annotation of the MDNs in the TEM reconstruction revealed bilateral arbors in the brain and
188 descending processes to abdominal segments (**Figure 4A**). Pre-synapses are restricted to the
189 descending processes (**Figure 4A, green**), whereas post-synapses are present in brain arbors
190 and descending processes, suggesting information flow from brain to VNC. A representative
191 MDN output synapse shown in **Figure 4B**; it is polyadic (multiple postsynaptic neurons
192 clustered around the MDN pre-synapse) and electron dense with associated presynaptic
193 vesicles.

Due to the ability of the MDNs to induce backward locomotion when activated, we focused on identifying MDN post-synaptic partners, with the goal of understanding the relationship between the MDN activation and motor output. The post-synaptic partners with the most synapses with MDN are: (1) the Pair1 SEZ descending neuron; (2) the thoracic descending neuron (ThDN); (3) the premotor neuron A18b; and (4) the MDNs themselves (**Figure 4C-D**). These are the top four MDN partners in both synapse number (**Figure 4C**) and percentage of total MDN output synapses (**Figure 4D**). All four MDNs have similar connectivity (Supplement to Figure 4). All of the top MDN output neurons are either premotor neurons or have preferential input into known premotor neurons (**Figure 4D-G**). For example, ThDN is strongly connected to A27l/A27k premotor neurons (**Figure 4C,E,H**), as well as to A18g which is not a premotor neuron. Pair1 is strongly connected to the previously described premotor neuron A27h (Fushiki et al., 2016), both directly and indirectly (**Figure 4C,F,J**). Lastly, A18b is a premotor neuron present in all abdominal segments, but it only receives MDN input in segment A1 (**Figure 4C,I**). Thus, the strongest output of the MDNs provides mono- and di-synaptic connectivity to premotor neurons. The activity and function of the MDN-A18b and MDN-Pair1 pathways in locomotion will be addressed below; we lack genetic tools to investigate the MDN-ThDN pathway.

There are numerous MDN inputs (an average of 396 post-synapses per MDN neuron) and we have not attempted to reconstruct them; this is beyond the scope of a single paper. However, we note that each MDN has similar inputs. We do not detect mono-synaptic sensory input into the MDNs (data not shown), but based on the requirement for MDNs to generate a backward crawl in response to a noxious head touch, we predict that there will be, minimally, polysynaptic connections from head mechanoreceptors to the MDNs.

MDNs activate A18b, a backward-active premotor neuron

The MDNs show anatomical connectivity to the A18b premotor neuron, which has not previously been characterized. We identified a LexA line that labels A18b within the VNC (R94E10, subsequently called A18b-LexA) along with a small, variable number of brain and thoracic neurons (Supplement to Figure 5). A18b has local, contralateral projections that match the morphology of A18b in the TEM reconstruction (**Figure 5A**), is cholinergic (**Figure 5B**), and is connected directly to the dorsal-projecting motor neurons aCC/RP2 and U1/U2 (**Figure 5C**) among other motor neurons.

We showed above that MDNs are significantly more active during backward than forward locomotion, raising the question of whether the A18b neurons are also preferentially active during backward locomotion. To answer this question, we performed three experiments. First, we used dual color calcium indicators in a fictive CNS preparation to simultaneously monitor motor neuron activity (GCaMP6m) and A18b activity (jRCaMP1b). We observed robust forward

and backward motor waves (**Figure 5D, top**), with A18b only active during backward motor waves, not forward motor waves (**Figure 5D, bottom**). Second, we performed dual color calcium imaging within intact larvae, and again observed that A18b was only active during backward motor waves (**Figure 5E**). Third, we used CaMPARI within intact larvae to determine if A18b was preferentially active during backward locomotion. We expressed CaMPARI in A18b and tested for activity-induced green-to-red photoconversion during either forward or backward locomotion. We found that illumination during forward locomotion generated minimal CaMPARI red fluorescence, whereas illumination during backward locomotion resulted in a significant increase in CaMPARI red fluorescence (**Figure 5F**). We call the A18b neuron backward-active rather than backward-specific because we do not know its pattern of activity in rolling or other larval behaviors. We conclude that A18b neurons are preferentially active during backward not forward locomotion.

To determine if MDNs activate A18b, we used Split1 to express Chrimson in MDNs and A18b-lexA to express GCaMP6f in A18b in fictive preparations. MDN stimulation led to a significant increase in GCaMP6f fluorescence in A18b, and this was not observed in controls lacking all-*trans* retinal (ATR), an essential co-factor for Chrimson function (**Figure 5G**). Interestingly, MDN activation triggered a backward wave of A18b activity from A2 to A6 (**Figure 5G**). We propose that MDN activates A18b in segment A1, which is the only segment we detect direct synaptic contacts, and this is transformed into an anterior-to-posterior wave of A18b activity.

We showed above that A18b has direct synaptic connectivity to motor neurons and is cholinergic, indicating that is likely to be an excitatory pre-motor neuron. Consistent with this expectation, we observed co-activity of A18b and motor neurons during backward motor waves in fictive preparations (**Figure 5H**), and found that A18b stimulation led to a significant increase in GCaMP6f fluorescence in motor neurons, which was not observed in controls lacking ATR (**Figure 5I**).

We wanted to test whether activation of A18b in segment A1 could induce backward waves of motor neuron activity. Unfortunately, the A18b-Gal4 line is not expressed in A1, precluding this experiment; moreover, it has “off-target” expression in the brain and in the VNC; these off-target neurons don’t prevent monitoring A18b activity because they don’t overlap with A18b arbors, but they make it impossible to selectively activate or silence A18b. In conclusion, our data support the following model: MDN activates A18b in segment A1, which initiates a coordinated anterior-to-posterior wave of A18b/motor neuron activity that drives backward locomotion.

MDNs activate Pair1, a backward-active descending interneuron

Connectomic data shows that MDNs are strongly connected to the bilateral Pair1 neurons, which send a descending projection to the VNC where they form synapses with A27h in posterior abdominal segments. A27h neurons are only active during forward locomotion (Fushiki et al., 2013). This leads to the hypothesis we test below: MDNs activate Pair1 to inhibit A27h, which terminates forward locomotion.

To determine if MDNs activate Pair1 we used Split1 to express Chrimson in MDNs, and R72C02-lexA (hereafter Pair1-lexA) (**Figure 6A**) to express GCaMP6f specifically in Pair1. Stimulation of MDNs led to a significant increase in Pair1 GCaMP6f fluorescence, and this was not observed in controls lacking ATR (**Figure 6B**). We conclude that the MDNs activate Pair1 neurons. In addition, we observed that every time MDNs were active, the Pair1 neurons were co-active (n=5; **Figure 6C**), although Pair1 could be active alone (n=5; Supplement to Figure 6). We conclude that MDNs activate the Pair1 neurons, and that other mechanisms exist for activating Pair1 as well.

We next used two methods to determine whether Pair1 neurons are preferentially active during backward locomotion. First, we used GCaMP6m to simultaneously monitor Pair1 and motor neuron activity in a fictive CNS preparation; this is possible because Pair1 and motor neuron processes are in different positions within the neuropil. These preparations show rhythmic forward and backward waves of motor neuron activity, and Pair1 neurons were only active during backward waves (100%, n=7 brains from which 53 backward waves were recorded; **Figure 6D**). Second, we expressed CaMPARI in Pair1 neurons and performed photoconversion during forward or backward locomotion. We found that illumination during forward locomotion generated a small amount of red fluorescence, whereas illumination during backward locomotion resulted in a significant increase in red fluorescence (**Figure 6E**). Taking all our anatomical and functional data together, we conclude that MDNs activate the A18b and the Pair1 neurons, which are both active specifically during backward but not forward locomotion.

Pair1 inhibits the A27h premotor neuron, arrests forward locomotion, and facilitates MDN-mediated backward locomotion

We confirm previous work showing that A27h is active during forward not backward locomotion (Fushiki et al., 2016)(Supplement to Figure 7A,B). This raises the interesting possibility that the MDNs coordinately switch locomotor behavioral states: concurrently promoting backward locomotion via A18b, and suppressing forward locomotion via Pair1 inhibition of A27h.

To test whether Pair1 inhibits the A27h neuron, we expressed Chrimson in Pair1 and GCaMP6m in A27h. We used Chrimson to stimulate Pair1 just as A27h activity was rising as part of a forward motor wave, and observed a significant decrease in A27h GCaMP6m fluorescence; this was not observed in controls lacking ATR (**Figure 7A,B**). Furthermore, we

found that Pair1 neurons are GABAergic (**Figure 7A''**), consistent with Pair1 direct repression of A27h activity. In addition, we found that Chrimson stimulation of Pair1 immediately and persistently blocked forward larval locomotion; control larvae lacking ATR briefly paused in response to illumination but rapidly resumed forward locomotion (**Figure 7C;** Movie 2). Consistent with an inhibitory relationship, we observed that Pair1 and A27h are not co-active (Supplement to Figure 7). We conclude that activation of the GABAergic Pair1 neurons inhibit A27h and prevent forward locomotion.

Our results suggest that Pair1 suppression of forward locomotion may be an essential component of MDN triggering a switch from forward to backward locomotion. If so, silencing Pair1 activity should reduce the effectiveness of MDN-induced backward locomotion; alternatively, MDN may be able to induce backward locomotion equally well without Pair1 function. Thus, we expressed Chrimson in MDNs and the neuronal silencer Shibire^{ts} in Pair1; Shibire^{ts} blocks vesicle release at 32°C but not at 25°C (experiment summarized in **Figure 7D**). We observed that silencing Pair1 alone had no effect on forward locomotion (**Figure 7E**, i-ii), but silencing Pair1 prior to low light or high light Chrimson-induced activation of MDN led to a loss in the effectiveness of MDN-induced backward locomotion (**Figure 7E**, iii-vi). We conclude that MDN triggers robust backward locomotion by coordinately activating the backward locomotion program and suppressing the forward locomotion program; we find no evidence for direct reciprocal inhibition between these pathways (Supplement to Figure 7D).

MDNs persist through metamorphosis and induce backward walking in adults

Larval MDNs share several features with the moonwalker descending neurons characterized in the adult (Bidaye et al., 2014; Sen et al., 2017). Both larval and adult neurons have anterior, medial somata with ipsilateral and contralateral arbors, and descending projections into the VNC. Both have presynaptic output into the SEZ and VNC. Could they be the same neurons? We tried to trace the MDNs through pupal stages using the Split1-Gal4 and observed the MDNs at early pupal stages (**Figure 8A**) and mid-pupal stages, where they began to prune their dendritic arbors (**Figure 8B**). However, Split1 was down-regulated by adulthood (data not shown), requiring us to use alternate methods to follow the larval MDNs into adulthood.

To permanently mark the larval MDN neurons, trace their morphology and test their gain of function phenotype in the adult brain, we used two distinct intersectional genetic methods. First, we generated an intersection between a larval MDN line and an adult MDN line to express the optogenetic activator ReaChr (genetics schematized in **Figure 8C**). If the larval MDNs become adult moonwalker neurons, they will express ReaChr:citrine and show light-induced backward walking. We observed light-induced backward walking in eight of ten adult flies assayed (**Figure 8D**; Movie 3); all eight had ReaChr::citrine expression in neurons matching the

342 moonwalker neuron morphology (**Figure 8E,F**), whereas the two flies that did not walk
343 backward also did not have ReaChr:citrine expression in moonwalker neurons (data not shown).
344 Second, we used 'immortalization' genetics (Harris et al., 2015) to permanently mark larval
345 MDNs and assay their function in the larva and adult (genetics schematized in **Figure 8G**). We
346 used Split1 to express an RU486-inducible FLP recombinase (hPR:FLP), allowing us to
347 chemically induce FLP activity in first instar larva when Split1 is only expressed in the MDNs
348 and a few off-targets. FLP activity resulted in permanent expression of lexA in the MDN
349 neurons, which immortalizes expression of *LexAop-Chrimson:Venus* in these neurons. We
350 identified larvae that crawled backward in response to Chrimson activation, and all grew into
351 adults that showed Chrimson-induced backward walking (n=20; **Figure 8H**). Importantly, all of
352 the backward walking adults that were successfully stained showed expression in the adult
353 moonwalker neurons (n=5; **Figure 8I,I'**); although each brain showed staining in a few
354 additional neurons (blue shading), only the MDNs were present in all of the brains.
355 We conclude that the larval MDNs are descending neurons that are born embryonically,
356 persist throughout larval stages, and survive into the adult. Surprisingly, activation of MDNs can
357 induce backward crawling in the limbless larva, as well as backward walking in the six-limbed
358 adult (**Figure 9A**). How much of the MDN larval circuitry persists into the adult is an interesting
359 open question (see Discussion).
360
361 **Discussion**
362
363 We have shown that MDNs are brain descending interneurons that activate two neuronal
364 pathways: one to stop forward locomotion, and one to induce backward locomotion (**Figure**
365 **9B,C**). This is similar to *C. elegans*, where in response to a head poke the ASH sensory neuron
366 activates AVA, a command neuron for backward locomotion (Lindsay et al., 2011), and
367 indirectly inhibits AVB, a command neuron for forward locomotion (Roberts et al., 2016),
368 although AVB inhibition may arise from reciprocal inhibition between AVA and AVB. It is also
369 similar to the role of the eighth nerve in simultaneously exciting the ipsilateral Mauthner neuron
370 while inhibiting, via a feed-forward inhibitory neuron, the contralateral Mauthner neuron
371 (Koyama et al., 2016). Our results raise the question of whether previously described
372 command-like neurons in *Drosophila* (Bidaye et al., 2014; King and Wyman, 1980; Sen et al.,
373 2017), leech (Kristan, 2008), lamprey (Dubuc et al., 2008), zebrafish (Kimura et al., 2013; Medan
374 and Preuss, 2014), mouse (Bouvier et al., 2015; Grillner and El Manira, 2015; Hagglund et al.,
375 2010; Jordan et al., 2008; Juvin et al., 2016; Roberts et al., 2008) and other animals may not
376 only induce a specific behavior, but concurrently inhibit an antagonistic behavior.
377 MDNs are required for backwards locomotion in response to mild noxious touch to the
378 head. It is unclear how the tactile sensory cue is transduced to the MDNs: we find no direct
379 sensory inputs to the MDNs in the current TEM connectome (data not shown). It is also

unknown whether MDNs are required for backward crawling in response to other noxious sensory modalities, such as high salt, bright light, or bitter taste. MDNs may be dedicated to responding to noxious mechanosensation, or they may integrate multimodal inputs to initiate backward locomotion.

The discovery of MDN command-like neurons that switch locomotion from forward to backward raises the question: are there command-like neurons that induce the opposite transition: from backward to forward locomotion? Whereas the MDN descending projection extends to A3-A5, and thus well past the thoracic and upper abdominal segments that initiate backwards locomotion (Berni, 2015; Heckscher et al., 2012; Pulver et al., 2015), a descending command-like neuron that induces forward locomotion is likely to project into the posterior abdominal segments, where forward waves are initiated (Berni, 2015; Heckscher et al., 2012; Pulver et al., 2015). Exploring the function of the latter type of descending neuron would help answer this question, as would the characterization of inhibitory inputs into the Pair1 or A18b backward-active neurons.

Our model is that activation of A18b in A1 induces backward locomotion. This model is based on several observations. (1) A18b is only active during backward locomotion. (2) MDN forms excitatory synapses on A18b in A1 but not more posterior segments. (3) Stimulation of MDN produces an A18b backward activity wave. (4) The A18b backward wave is always concurrent with a motor neuron backward wave. Unfortunately, we are unable to directly test the function of A18b in triggering backward locomotion due to the A18b Gal4 line having off-target expression in the brain and in the VNC, and lacking expression in A1 or thoracic segments (Supplement to Figure 5). Backward motor waves are initiated from the thorax (Pulver et al., 2015), and it is likely that stimulation of A18b in A1 or thoracic segments would be required to induce a backward motor wave. In support of this notion, the A02o “wave” neuron can only induce backward motor waves following stimulation in anterior abdominal segments (Takagi et al., 2017). The relationship between A18b and A02o is unclear (they are not directly connected), nor is it known how activation of either produces a backward motor wave. This level of understanding would require a comprehensive anatomical and functional analysis of larval premotor and motor circuits.

We propose that MDNs directly excite Pair1 neurons to halt forward locomotion. But there are also additional mechanisms to induce Pair1 activity, as many Pair1 activity bouts occur without MDN activity. It appears that backward locomotion can be induced via MDN-dependent or -independent pathways, and both show correlated Pair1 activity. The inputs in addition to MDN that activate Pair1 during backward locomotion remain to be discovered.

The least understood MDN output to motor neurons is the MDN-ThDN-A27k/l pathway. A27l is inhibitory (AAZ and CQD, unpublished) so if ThDN is also inhibitory, it would provide a disinhibitory circuit motif for activating A18b. This would be synergistic with MDN direct excitation of A18b. There are currently no genetic tools providing access to ThDN or A27k

418 neurons, and the existing driver line for A27l has off-target neurons, precluding a functional
419 analysis of this pathway.
420 MDNs can induce backward crawling in the limbless *Drosophila* larva, and persist into
421 adulthood where they can induce backward walking in the six-legged adult fly. This is
422 remarkable, because most mechanosensory neurons are completely different (Kendroud et al.,
423 2018; Kernan, 2007), although there are some gustatory and stomatogastric sensory neurons
424 that survive from larva to adult (Kendroud et al., 2018). Similarly, most or all of the downstream
425 motor neurons controlling crawling (larva) and walking (adult) are different: abdominal motor
426 neurons in the larva and thoracic motor neurons in the adult. It will be interesting to see which,
427 if any, interneurons in the larval MDN circuit remain connected in the adult, and whether they
428 perform the same function in the adult. For example, does the larval Pair1-A27h circuit persist
429 in the adult, but become restricted to thoracic segments? It is also interesting to consider the
430 evolution of the MDN circuit; some of the neurons we describe here may originally have been
431 used to regulate adult walking, prior to becoming co-opted for regulating larval crawling.
432
433

Materials and Methods

Transgenes

pBDP-Gal4 in attP2 (gift from B.D. Pfeiffer, JRC)
pBDP-LexA:p65Uw in attp40 (gift from T. Shirangi, Villanova Univ)
R53F07-Gal4 (BDSC# 50442)
R53F07-Gal4^{DBD} (Doe lab)
R49F02-Gal4^{AD} (a gift from G. Rubin, JRC)
R94E10-Gal4 (A18b line; BDSC# 40689)
R94E10-lexA (A18b line; Doe lab)
R36G02-Gal4 (A27h line; BDSC# 49939)
R75C02-Gal4 (Pair1 line; BDSC# 39886)
R75C02-lexA (Pair1 line; a gift from M. Louis, UC Santa Barbara)
ss01613-Gal4 (Split3; a gift from M. Louis, UC Santa Barbara and J. Truman, Univ. Washington)
CQ2-lexA (U1-U5 motor neurons; Doe lab)
RRa-Gal4 (aCC/RP2 motor neurons; a gift from M. Fujioka, Thomas Jefferson Univ.)
tsh-lexA (a gift from J. Simpson, UC Santa Barbara)
UAS-Chrimson:mCherry (a gift from V. Jayaraman, JRC)
UAS-Chrimson:mVenus (BDSC# 55138)
UAS.dsFRT.Chrimson:mVenus (a gift from G. Rubin, JRC)
UAS-MCFO2 (BDSC# 64086)
UAS-GCaMP6m (BDSC# 42748)
UAS-GCaMP6f (a gift from V. Jayaraman, JRC)
UAS-jRCaMP1b (BDSC# 63793)
lexAop-GCaMP6f (gift from V. Jayaraman, JRC)
lexAop-Gal80 (BDSC# 32213)
lexAop-Chrimson:mCherry (a gift from V. Jayaraman, JRC)
lexAop-KZip+:3xHA (a gift from B. White, NIH)
UAS-CaMPARI (BDSC# 58761)
UAS-GtACR1 (a gift from A. Claridge-Chang, Duke-NUS Med School)
lexAop-shibire^{ts} in attP2 (a gift from G. Rubin, JRC)
VT044845-lexA (adult moonwalker line; a gift from B. Dickson, JRC)
hsFlpG5.PEST (BDSC# 62118)
pJFRC108-20XUAS-IVS-hPR:Flp-p10 (a gift from J. Truman, Univ. Washington)
Actin5C-FRT>-dSTOP-FRT>-LexAp:65 (a gift from J. Truman, Univ. Washington)
P[13XLexAop2-IVS-CsChrimson.mVenus] attP18 (BDSC# 55137)
lexAop-(mCherry-STOP-FRT) ReaChR:Citrine VK00005 (BDSC #53744)

Fly stocks

Split1 (*R53F07-Gal4^{DBD} R49F02-Gal4^{AD}*)
Split2 (*R53F07-Gal4^{DBD} R49F02-Gal4^{AD} tsh-lexA lexAop-KZip+:3xHA*)
Split3 (*ss01613-Gal4*)
Immortalization stock: *P[13XLexAop2-IVS-CsChrimson.mVenus]attP18; Actin5C-FRT-STOP-FRT-lexAop::65; pJFRC108-20XUAS-IVS-hPR::Flp-p10*

Immunostaining and imaging

Standard confocal microscopy, immunocytochemistry and MCFO methods were performed as previously described for larvae (Clark et al., 2016; Heckscher et al., 2015) or adults (Nern et al., 2015; Pfeiffer et al., 2008). Primary antibodies used recognize: GFP or Venus (rabbit, 1:500, ThermoFisher, Waltham, MA; chicken 1:1000, Abcam13970, Eugene, OR), GFP or Citrine (Camelid sdAB direct labeled with AbberiorStar635P, 1:1000, NanoTab Biotech., Gottingen, Germany), GABA (rabbit, 1:1000, Sigma, St. Louis, MO), mCherry (rabbit, 1:1000, Novus, Littleton, CO), Corazonin (rabbit, 1:2000, J. Veenstra, Univ Bordeaux), FasII (mouse, 1:100, Developmental Studies Hybridoma Bank, Iowa City, IA), HA (mouse, 1:200, Cell signaling, Danvers, MA), or V5 (rabbit, 1:400, Rockland, Atlanta, GA), Flag (rabbit, 1:200, Rockland, Atlanta, GA). Standard methods were used for pupal staging (Bainbridge and Bownes, 1981). Secondary antibodies were from Jackson Immunoresearch (West Grove, PA) and used according to manufacturer's instructions. Confocal image stacks were acquired on Zeiss 700, 710, or 800 microscopes. Images were processed in Fiji (https://imagej.net/Fiji), Adobe Photoshop (Adobe, San Jose, CA), and Adobe Illustrator (Adobe, San Jose, CA). When adjustments to brightness and contrast were needed, they were applied to the entire image uniformly. Mosaic images to show different focal planes were assembled in Fiji or Photoshop.

Electron microscopy and CATMAID

We reconstructed neurons in CATMAID using a Google Chrome browser as previously described (Ohyama et al., 2015). Figures were generated using CATMAID graph or 3D widgets.

Chrimson and GtACR behavioral experiments

Embryos were collected for 4 h on standard 3.0% agar apple juice collection caps with a thin layer of wet yeast, and transferred to standard cornmeal fly food supplemented with 0.5mM all-*trans* retinal at 48 hours after collection. Following another 48 hours (96 +/-6 h larval age) animals were collected and transferred to 3.0% agar apple juice caps and relocated to the room were behavioral data was collected. Five minutes after acclimation to the room, one animal at a time was transferred to of 3.0% agar apple juice square arenas, 2 cm thick with an area of 81.0cm^2, and crawling was then recorded at 5 Hz using an Axiocam 506 mono under low transmitted light from bellow for 15 s follow by 15 s under 0.275 mW/mm^2 green light. Temperature of the room was kept at 24+/-2C°. Number of forward waves and backward waves, and percent of time engaged in either forward, backward or paused were manually quantified using the recorded movies. Unpaired Student's t-test was performed to ask significance in the number of waves over 15 s.

The Chrimson together with Shibire silencing experiment (Figure 7F-G) was performed as the Chrimson only experiments described above except that the agar arena was placed on top of a heating plate which was kept at 25C° or at 32C° for Shibire Off or On groups respectively. Animals were individually placed on the arena. After 1 minute to reach the desired temperature we manually quantified the number of forward and backward waves with no light, under 0.07 mW/mm^2 green light or 0.275 mW/mm^2 green light.

For GtACR1 experiments (Figure 1G-H), instead of square arenas, animals were placed into a 0.75mm wide agar lane to limit their movement to forward or backward locomotion only. To quantify backward wave probability (Figure 1G) larvae were gently poked in the most anterior part of their body and scored whether the animal responded with backward crawling (regardless of how many backward peristaltic waves). We then calculated the probability by dividing the number of times the animal began backward crawling immediately after a poke by the total number of times that each animal was poked, which was always 5 times. For each animal this was done with no light first and then under 0.96 mW/mm^2 green light. We performed one-way ANOVA with Bonferroni post-hoc test between light ON groups. For panel 1H we induced a backward run and turned on the 0.96 mW/mm^2 green light immediately after the second backward wave. We define a backward run as two or more consecutive backward peristaltic waves after being poked

in the most anterior part of the animal. We scored how many backward waves animals performed after the light was turned on.

Calcium Imaging

For dual-color and single-color calcium imaging in fictive preps, freshly dissected brains were mounted on 12mm round Poly-D-Lysine Coverslips (Corning® BioCoat™) in HL3.1 saline, which were then were placed on 25 mm × 75 mm glass slides to be imaged with a 40× objective on an upright Zeiss LSM-800 confocal microscopy. To do calcium imaging in intact animals (Figure 5E), a second or third instar larva was washed with distilled water, then moved into a drop of halocarbon oil 700 (Sigma, St. Louis, MO) on the slide. A 22 mm × 40 mm cover glass was put on the larva and pressed gently to restrict larval locomotion. The larva was mounted ventral side up so that the ventral nerve cord could be imaged using 40× objective on an upright Zeiss LSM800 confocal microscope. To simultaneously image GCaMP6m and jRCaMP1b, signals in non-overlapping regions of interest (ROI) were imaged with 488 nm and 561 nm diode lasers. The images were imported to FijI (https://imagej.net/fiji) by which GCaMP6m and jRCaMP1b channels were separated. The $\Delta F/F_0$ of each channel was calculated as $(F-F_0)/F_0$, where F_0 was averaged over ~1s immediately before the start of the forward or backward waves in each ROI.

Functional connectivity assays

Freshly dissected brains were mounted in HL3.1 saline as described above, with the exception that the dissection was done under the minimum level of light possible to prevent activation of Chrimson. GCaMP6m or GCaMP6f signal in postsynaptic neurons were imaged using 2-4% power of the 488nm laser with a 40× objective on an upright Zeiss LSM800 confocal microscope. Chrimson in presynaptic neurons was activated with three pulses of 561 nm laser at 100% power delivered via the same 40× objective using the bleaching function in the ZEN Zeiss software. The total length of the pulses carried depend on the ROI size which was kept consistent across ATR+ and ATR– samples within an experiment. For A18b activation (Figure 5I), the light pulse was 700 msec; for MDN activation (Figure 6B) and Pair1 (Figure 7B), the light pulse was 440 msec. To quantify $\Delta F/F_0$ traces we used MATLAB. Before extracting any fluorescence our script first performs rigid registration to correct for movement while recording. F_0 was set as the average fluorescence of the 3 frames acquired before each Chrimson stimulus analyzed. For predicted excitatory connections (Figure 5I and 6B), we first average $\Delta F/F_0$ traces for two consecutive 561nm Chrimson stimuli separated by 20 488nm acquisition frames. This was enough time to let GCaMP6f levels back to ground state. For predicted inhibitory connections (Figure 7B), we gave multiple 440 msec Chrimson stimuli separated by 5 seconds. After recording, we then selected all events where the start of the Chrimson stimulus coincided with an A27h forward activity wave, which was necessary to elevate the GCaMP6m levels sufficiently to see subsequent Chrimson-induced inhibition. We selected the A27h segmental neuron with the highest mean fluorescent intensity in the frame before the Chrimson stimulus from segments A4-A7 (where Pair1 synapses with A27h). For all Chrimson experiments, traces were averaged across animals.

CaMPARI experiments

Larvae were collected 96hrs days after egg laying and place in agar apple collection caps for at least 5 min to acclimate animals to the environment. Using a soft brush, larvae were placed into a 0.75mm wide agar lane to limit their movement to forward or backward locomotion only. We let the animals start crawling forward for at least 5 seconds in the lanes. For forward data collection, the photoconvertible 405nm light was turned on at 0.5mW/mm^2 while the larvae crawled forward for 30 sec. For backward, same light was turned on and backward locomotion was immediately induced by gentle touch on the most anterior part of the larva with a semi-blunt pin. Brains were dissected in HL3.1, then green and red CaMPARI signals were imaged with a 40× objective on Zeiss LSM-800 confocal microscope in the

regions of interest. ROIs were manually selected using the green channel. Fluorescence within ROIs were quantified using Image J.

Adult behavioral intersectional experiment (Figure 8 F-I)

After eclosion adults were transferred to standard cornmeal fly food supplemented with ATR (0.5mM) for 4 days changing to fresh food after two days. Wings were clipped and animals were placed in ring arenas made of 3.0% agar apple juice. The ring arena size was 1.4cm outer diameter, 1.0cm inner diameter and 0.2cm height. After 5 minutes for environmental acclimation, animal behavior was recorded at 5 Hz using an Axiocam 506 mono under low transmitted light for 10 seconds followed by 10 seconds under 0.28 mW/mm^2 red light. This was done three times for each animal. To quantify backward locomotion probability upon light stimulus we divided the amount of times the animal began backward walking within 2 seconds after light stimulus over the total number of times the animals was presented with light. To calculate significance we used Student's t-test unpaired analysis.

Adult behavior immortalization with RU486 experiment(Figure 8J-L)

Adult flies were allowed to lay eggs on standard culture medium that was supplemented with 1μM RU486 and 2mM ATR. After 24 hours, light-induced backwards crawling larvae were transferred to culture medium supplemented with 2mM ATR and grown to adulthood. 2-6 day-old adult flies were individually transferred into a 10ml serological pipette for walking assay. Red-orange light from a 617nm high-power LED was fiber-coupled to a 200μm core optical cable that was manually triggered via a T-Cube LEDD1B driver (ThorLabs, Newton, NJ, USA). Optogenetic stimulation was measured via a photodiode power sensor (S130VC, ThorLabs) to be ~4.6 $\mu W/mm^2$. We performed same analysis for the intersectional experiment (above) to quantify backward locomotion probability upon light stimulus.

Statistical analysis

Statistical significance is denoted by asterisks: ****p<0.0001; ***p<0.001; **p<0.01; *p<0.05; n.s., not significant. All statistical Student's t-tests were performed using Graphpad Prism software. One way ANOVA with Bonferroni post-hoc test was done using http://astatsa.com/. The results are stated as mean ± s.d., unless otherwise noted.

Acknowledgements

We thank Jim Truman and Matthieu Louis for unpublished fly lines targeting MDN and Pair1 neurons. We thank Brandon Mark for MATLAB scripts. We thank Todd Laverty, Gerry Rubin, Barry Dickson, Ben White, Miki Fujioka, Julie Simpson and Adam Claridge-Chang for fly stocks, and Barry Dickson, Shawn Lockery, Matthieu Louis, and Tory Herman for comments on the manuscript. We thank Avinash Kandelwal and Laura Herren for annotating neurons, and Keiko Hirono for generating transgenic constructs. Transgenic lines were generated by BestGene (Chino Hills, CA) or Genetivision (Houston, TX). Stocks obtained from the Bloomington Drosophila Stock Center (NIH P40OD018537) were used in this study. Funding was provided by HHMI (CQD, AC-R, AAZ, LM), NIH HD27056 (CQD, MQC), F32NS105350-01A1 (AC-R), T32HD007348-24 (MQC), and T32GM007413-36 (MQC).

Author contributions

MQC conceived of the project; MQC, LM, AC-R, AAZ performed experiments; RF generated the ssTEM volume; AAZ and AC annotated neurons in CATMAID; MQC, AC-R, AAZ, AC and CQD wrote the paper. All authors commented and approved of the manuscript.

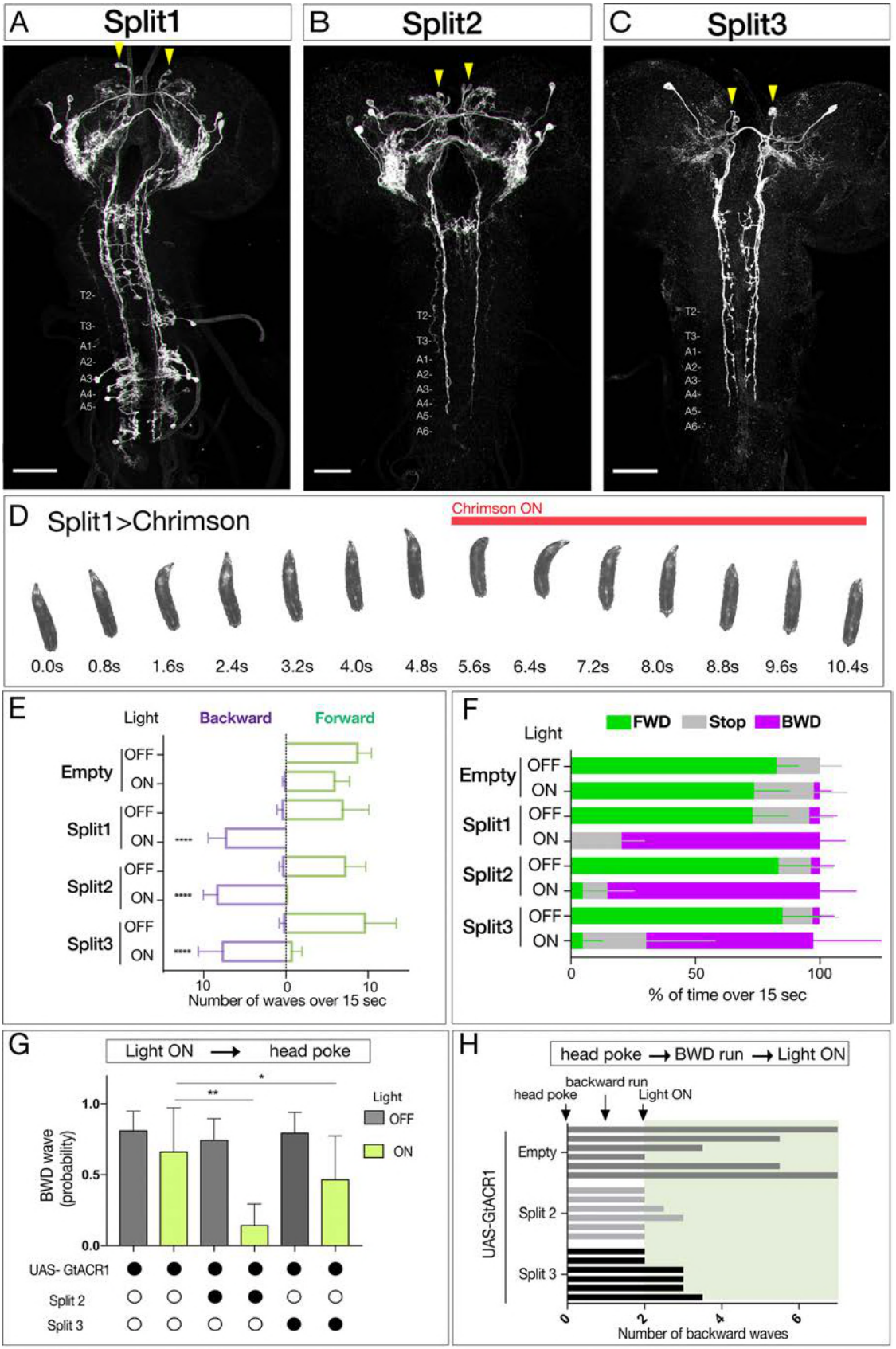

Figure 1

619

Figure 1. Neurons sufficient to induce backwards locomotion in third instar larvae

(A-C) Split1-Split3 lines driving expression of membrane localized Venus in the third instar CNS. Corazonin (not shown) labels a single neuron in segments T2-A6, and was used to identify VNC segment identity. The only neurons potentially common to all three lines are a pair of bilateral ventral, anterior, medial neurons (arrowheads). Maximum intensity projection of entire CNS shown. Anterior, up; scale bars, 50µm. Genotypes: *R49F02-Gal4^{AD} R53F07-Gal4^{DBD} UAS-Chrimson:mVenus* (Split1); *R49F02-Gal4^{AD} R53F07-Gal4^{DBD} tsh-lexA lexAop-killer zipper UAS-Chrimson:mVenus* (Split2); *ss01613-Gal4 UAS-Chrimson:mVenus* (Split3).

(D) Split1 activation induces backwards locomotion. Genotype: *R49F02-Gal4^{AD} R53F07-Gal4^{DBD} UAS-Chrimson:mVenus*.

(E) Split1, Split2, or Split3 activation induces backward locomotion. Number of backward or forward waves in third instar larvae over 15s with or without Chrimson activation. N = 10 for all genotypes. Genotypes: *pBD-Gal4 UAS-Chrimson:mVenus* (Empty) and see A-C above for Split1-3 genotypes.

(F) Split1, Split2, or Split3 activation induces backward locomotion. Percentage of time performing forward locomotion (green), backward locomotion (magenta) or paused (grey) in third instar larvae over 15s with or without Chrimson activation. N = 5 for all genotypes. Genotypes, see A-C.

(G) Split2 or Split3 silencing reduces initiation of backward locomotion. Backward waves induced by a noxious head poke, with or without active GtACR1. Genotypes: *pBD-Gal4 UAS-GtACR1:mVenus* (first two bars, n= 20), *R49F02-Gal4^{AD} R53F07-Gal4^{DBD} tsh-lexA lexAop-killer zipper UAS-GtACR1:mVenus* (middle two bars, n = 8), *ss01613-Gal4 UAS-GtACR1:mVenus (*last two bars, n = 25).

(H) Split2 or Split3 neuron silencing stops ongoing backward locomotion. After each larva initiated a backward run (two backward waves), light was used to activate GtACR1 or a no Gal4 control, and the number of backward waves was counted. n=6 for both groups; each bar represents the average of two trials for the same larva. See G for genotypes.

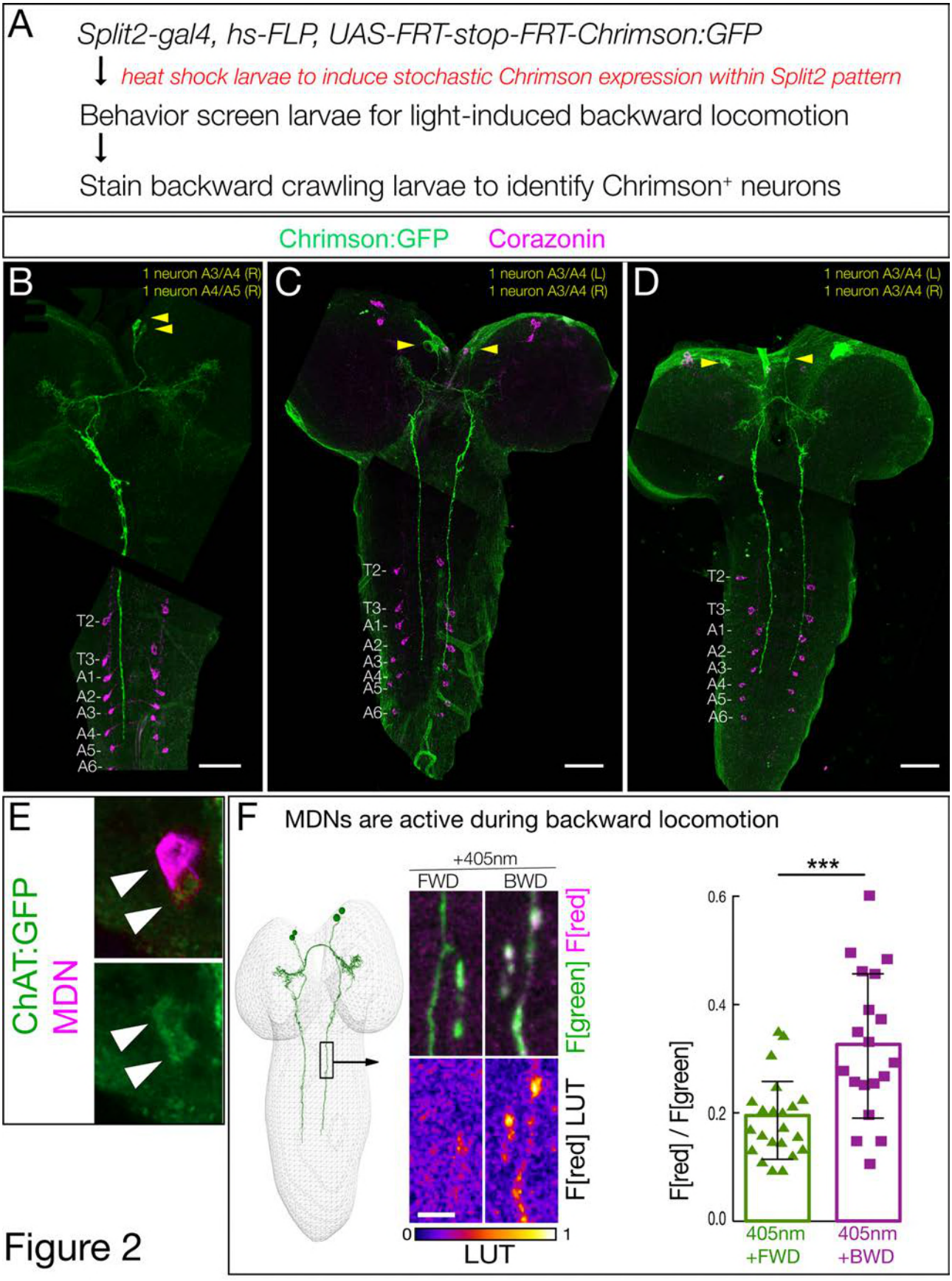

Figure 2

643

644 **Figure 2. Two brain descending neurons are sufficient to induce backward larval locomotion**
645 (A) Experimental flow for generating sparse, stochastic patterns of Chrimson in subsets of the Split2 expression
646 pattern. Genotype: *hsFlpG5.PEST R49F02-Gal4^{AD} R53F07-Gal4^{DBD} tsh-lexA, lexAop-killer zipper*
647 *UAS.dsFRT.Chrimson:mVenus*.
648 (B-D) The CNS from three larvae that crawled backward in response to Chrimson activation. All show expression in
649 neurons with medial cell bodies, bilateral arbors, and a contralateral descending projection to A3-A5. (B) Note there
650 is a tear in the CNS near segment T1. Chrimson:Venus, green; Corazonin (Crz; segmental marker), magenta. Scale
651 bar, 50 µm.
652 (E) MDNs are cholinergic. MDNs marked with mCherry (magenta) express ChAT:GFP (green). Genotype: *R49F02-*
653 *Gal4^{AD},UAS-Chrimson:mCherry; R53F07-Gal4^{DBD}, mimic ChAT:GFP*.
654 (F) MDNs are preferentially active during backward (BWD) not forward (FWD) locomotion in the intact larva.
655 CaMPARI in MDN descending projections within the SEZ of third instar larvae. Top, fluorescence emission following
656 excitation by 488nm (green) or 561nm (magenta); bottom, emission from 561nm imaging alone. Right,
657 quantification of red fluorescence over green fluorescence, mean intensity. Each value represents data from an
658 individual descending projection. See methods for details. n= 22 for FWD and 19 for BWD. Scale bar, 10 µm.
659 Genotype: *R49F02-Gal4^{AD} R53F07-Gal4^{DBD} UAS-CaMPARI*.
660
661

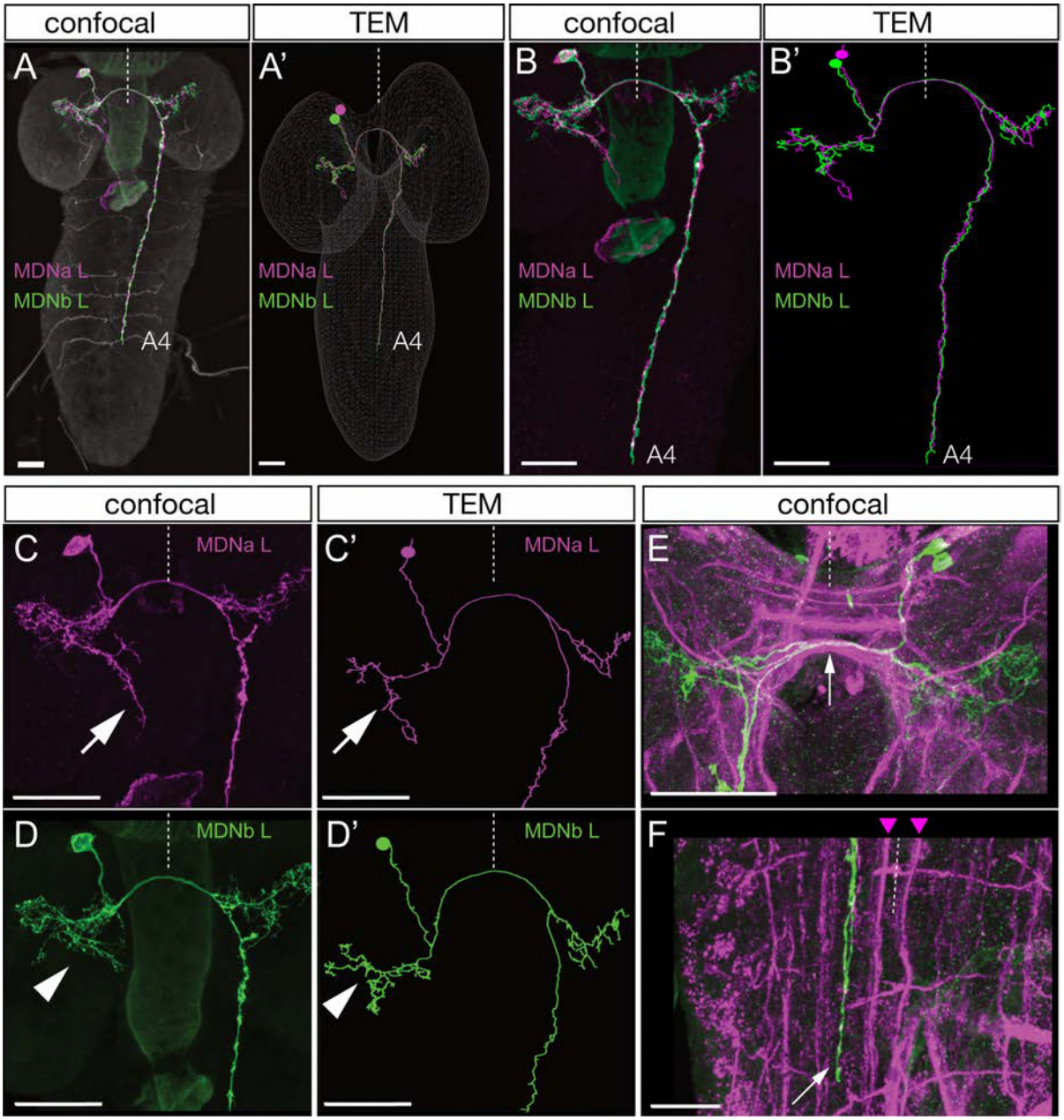

Figure 3. Identification of Mooncrawler Descending Neurons by light and electron microscopy

(A-F) Light microscopy. Multicolor FLP-out (MCFO) was used to visualize the morphology of individual neurons in the Split2 pattern in first instar larvae. Two neurons show morphology matching that seen in the Chrimson FLP-out experiments in Figure 2. Both neurons have anterior medial somata (A), ipsilateral and contralateral arbors (A-D), a contralateral projection in the posterior commissure (E, arrow), and descending neurons terminating in segments A3-A5 of the VNC (A-B). The neurons run lateral to the dorso-medial (DM) FasII tract in the VNC (F, DM tract marked with arrowheads). The two neurons can be distinguished by their ipsilateral arbor, which is either linear (C, arrow) or bushy (D, arrowhead).

(A'-D') Reconstructions from serial section transmission electron microscopy (TEM) of a first instar larva. Two neurons indistinguishable from the MDNs can be identified in the TEM reconstruction: MDNa (linear ipsilateral arbor) and MDNb (bushy ipsilateral arbor). We simply call them MDNs due to their similar morphology and connectivity. All panels show dorsal views with midline indicated (dashed line). Scale bars, 20 µm.

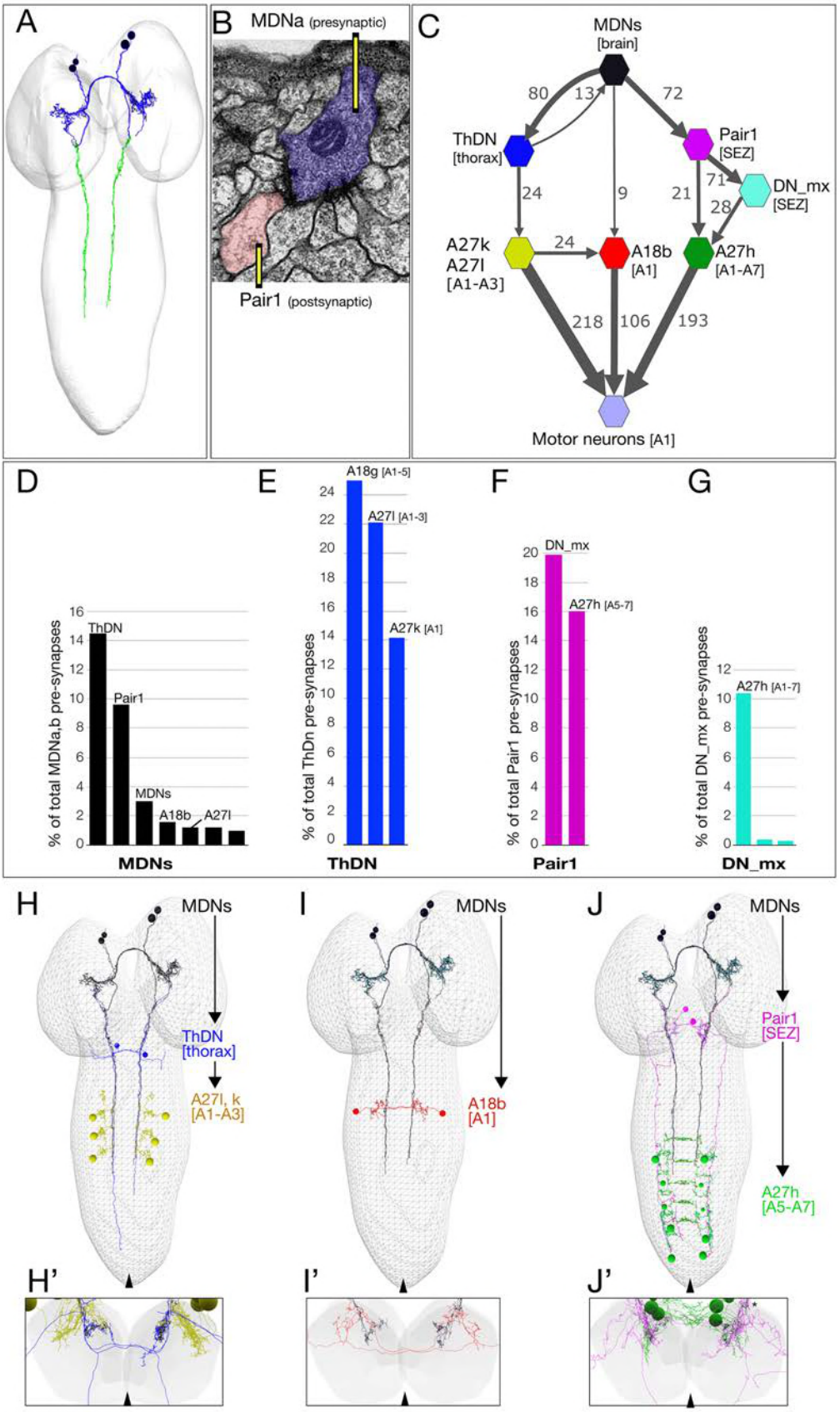

Figure 4

676

677 **Figure 4. The MDN connectome: three pathways to distinct subsets of premotor neurons**
678 (A) TEM reconstruction of the bilateral MDNa,b neurons. Neuronal skeletons are colored to show post-synapses in
679 the presumptive dendritic arbors of the brain (blue) and pre-synapses in the presumptive axonal descending process
680 (green). Anterior, up.
681 (B) Representative MDN output pre-synapse (blue) onto a post-synaptic Pair1 neuron (pink).
682 (C) MDNs and their strongest post-synaptic partners (synapse number shown next to connection arrows, and line
683 width is proportional to synapse number). All connectivity is shown except unilateral synapses, <6 synapses, and the
684 15 synapses between MDNs. Each polygon represents pairs of the indicated neuron with the exception of these
685 larger groups: A27k/A27l (six A27l neurons in A1-A3, four A27l neurons in A1-A2); A27h (14 neurons in A1-A7), and
686 30 pair of motor neurons in A1. This graph is provided as Supplemental File1.json that can be opened in CATMAID.
687 (D-G) Quantification of the percent of total pre-synapses that are targeted to the indicated neuron. All connectivity
688 is shown except unilateral or <5 synapse connections.
689 (H-J) The three MDN to premotor neuron pathways. (H) MDN-ThDN-A27l/k pathway. Only A27l is shown; A27k has a
690 very similar morphology. (I) MDN-A18b pathway. (J) MDN-Pair1-A27h pathway. Dorsal view; anterior, up; midline,
691 arrowhead.
692 (H'-I') Respective cross-sectional view of VNC neuropil (gray) and neurons in each pathway; note that synapses are
693 primarily in the dorsal (motor) neuropil. Dorsal up, midline, arrowhead. Asterisk in J' shows the approximate site of
694 the synapse shown in panel B.
695
696

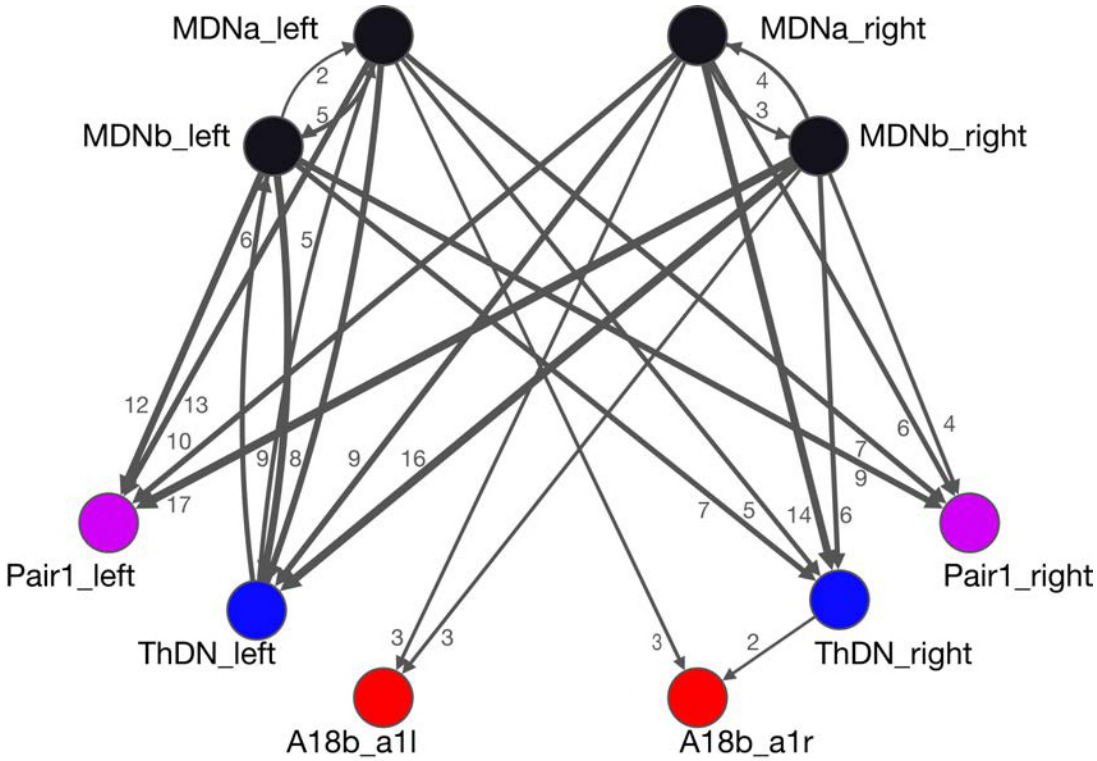

Supplement to Figure 4. All MDNs have similar connectivity.

All synapses between the MDNs and output target neurons are shown, except those with single synapse connectivity. All MDNs have similar input connectivity as well (data not shown).

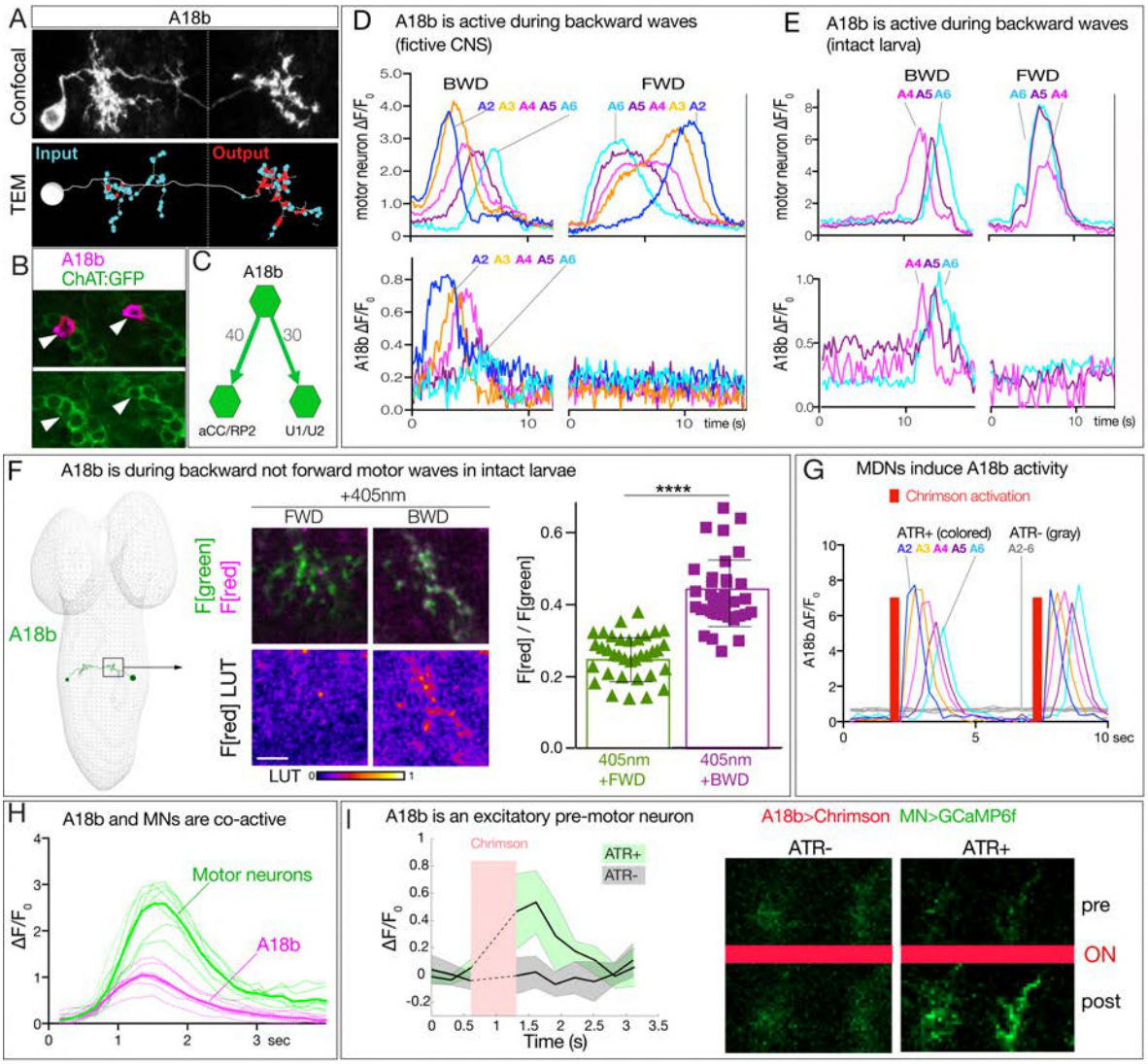

Figure 5

706

Figure 5. MDN activates the excitatory backward-active A18b premotor neuron.

(A) A18b morphology by light (MCFO) and electron microscopy (TEM). Top: Dorsal view of an individual A18b neuron in a second instar larval CNS by light microscopy (R94E10 > MCFO). Bottom: Dorsal view of an individual A18b neuron in a first instar larva in the TEM reconstruction. Cyan dots, post-synaptic sites; red dots, pre-synaptic sites. Anterior, up. Midline, dashed line.

(B) A18b is cholinergic. A18b cell body (mCherry; magenta) and ChAT:GFP (green). Genotype: *R94E10-Gal4, UAS-Chrimson:mCherry; mimic ChAT:GFP*.

(C) Connectivity of A18b to the dorsal-projecting motor neurons aCC/RP2 and U1/U2 in segment A1 from the TEM reconstruction. Synapse number shown.

(D) In fictive preparations, A18b neurons are active in backward but not forward locomotion. $\Delta F/F_0$ of GCaMP6m in U1-U5 motor neurons (top) or jRCaMP1b in A18b (bottom) of five segments executing a forward (FWD) and then a backward (BWD) wave. This experiment was performed on 8 different isolated third instar CNSs with similar results. Genotype: *CQ-lexA/+; lexAop-GCaMP6m/R94E10-Gal4 UAS-jRCaMP1b.*

(E) In intact larvae, A18b neurons are active in backward but not forward locomotion. $\Delta F/F_0$ of GCaMP6m in motor neurons (top) and jRCaMP1b in A18b (bottom) in three segments. Times of BWD and FWD motor waves indicated. This experiment was performed on 19 waves (11 BWD, 8 FWD) in 7 third instar larvae, all with similar results. Genotype: *CQ-lexA/+; lexAop-GCaMP6m/R94E10-Gal4 UAS-jRCaMP1b*

(F) In intact larvae, A18b is preferentially active during backward not forward locomotion. CaMPARI in A18b neurites in a third instar larval CNS. Top, fluorescence emission (F) following 488nm (green) or 561nm (magenta) illumination; bottom, emission from 561nm alone. Left, photoconversion (405nm) during FWD or BWD locomotion. Right, quantification of red fluorescence over green fluorescence mean intensity. Each value represents data from an individual neurite. n= 35 for FWD and 36 for BWD. LUT, 561nm emission intensity look up table. Scale bar, 10µm. Genotype: *R94E10-Gal4 UAS-CaMPARI*.

(G) In fictive preparations, MDNs activate A18b neurons, and induce backward A18b activity waves. Chrimson is expressed in MDN, and GCaMP6f in A18b. Red bars, time of 561 nm Chrimson activation. Colored traces indicate the $\Delta F/F_0$ of A18b GCaMP6f signal in 5 segments of an ATR+ brain; gray traces are from ATR- animal. This experiment was performed on 5 different animals with similar results. Genotype: *R49F02-Gal4^{AD}/R94E10-lexA; R53F07-Gal4^{DBD}/lexAop-GCaMP6f UAS-Chrimson:mCherry*.

(H) In fictive preparations, A18b fires synchronously with motor neurons during backward waves. Dual color calcium imaging of jRCaMP1b in A18b (red) and GCaMP6m in U1-U5 motor neurons (green). Dotted traces, activity during individual BWD waves in seven segments from 3 animals; solid traces, average. Genotype: *CQ-lexA/+; lexAop-GCaMP6m/R94E10-Gal4 UAS-jRCaMP1b*.

(I) A18b is an excitatory pre-motor neuron. A18b expresses Chrimson and aCC/RP2 motor neurons express GCaMP6f. Left: $\Delta F/F_0$ traces of GCaMP6f before and after 561 nm Chrimson activation (red bar) of three aCC/RP2 axons/dendrites within an animal. Solid bars represent means and shaded regions represent standard deviation from the mean (SDM). ATR+ is shaded in green and ATR- in grey. Five animals were used in each group. GCaMP6f signal was not acquired during the Chrimson activation (dashed lines); t-test analysis for the first $\Delta F/F_0$ value after Chrimson activation between +ATR and -ATR showed significance (p=0.0071). Right: images of motor neuron GCaMP6f fluorescence pre- and post-Chrimson activation in ATR+ and ATR- larvae. Genotype: *94E10-lexA/+; lexAop-Chrimson:mCherry/RRa-Gal4 UAS-GCaMP6f.*

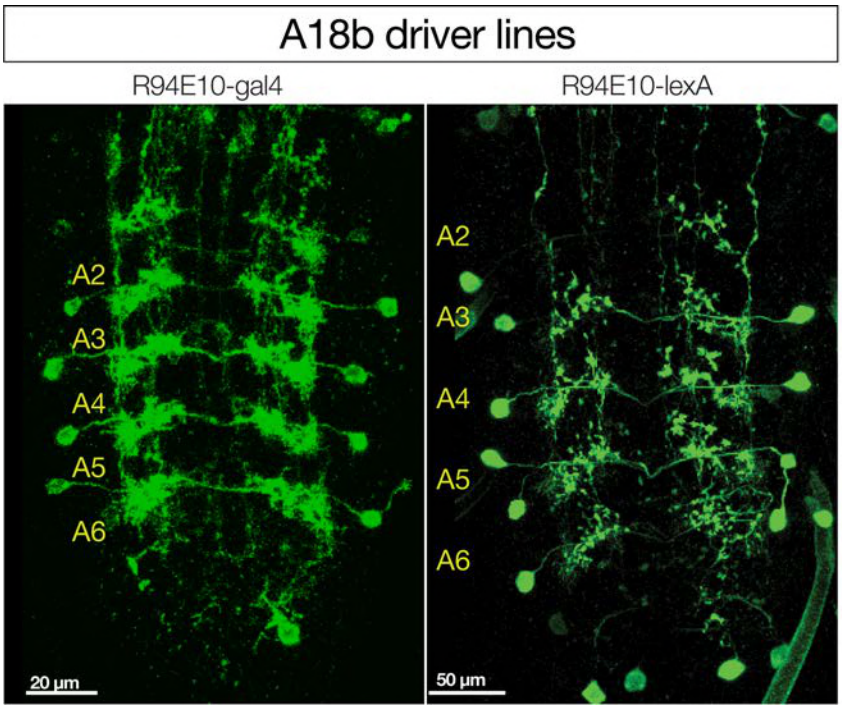

Supplement to Figure 5. Driver lines for A18b.

R94E10-Gal4 and R94E10-LexA expression in A18b (shown); in addition, both lines have off-target expression in the brain (~10 neurons) and more medially in the VNC (~3 neurons) that are not shown. Note that both lines lack expression in A18b in A1 where MDNs form synaptic contacts, thus the increase in GCaMP6f fluorescence observed following MDN activation is either due to A18b activation in A1 triggering a posterior wave of A18b activity, or another indirect pathway. Dorsal view; anterior up.

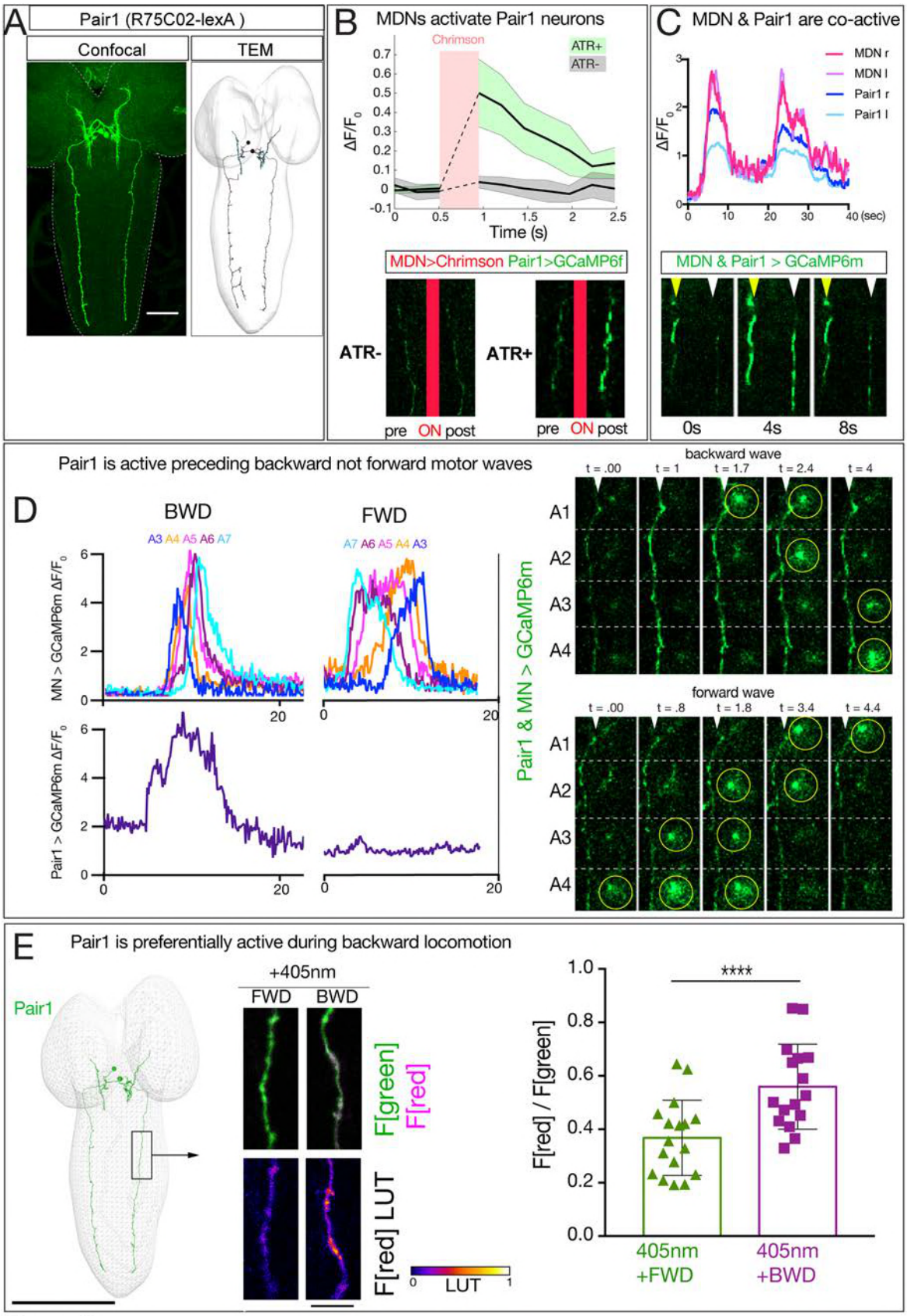

Figure 6

760

761 **Figure 6. MDN activates Pair1 which is a backward-active descending neuron.**
762 (A) Pair1 neurons by light (confocal) and electron microscopy (TEM). Confocal image is an L3 CNS, TEM
763 reconstruction is from an L1 CNS. Anterior, up. Scale bar, 50 µm. Genotype: *R72C02-lexA lexAop-myr:GFP.*
764 (B) MDNs activate Pair1. MDN expresses Chrimson and Pair1 neurons express GCaMP6f. Top: $\Delta F/F_0$ traces of
765 GCaMP6f before and after Chrimson activation (red bar) of Pair1 axons. Solid bars represent means and shaded
766 regions represent standard deviation from the mean (SDM). ATR+ is shaded in green and ATR- in grey. Six animals
767 were used for ATR+ and five for ATR-. GCaMP6f signal was not acquired during the Chrimson activation (dashed
768 lines); t-test analysis for the first $\Delta F/F_0$ value after Chrimson activation between +ATR and -ATR showed significance
769 (p =0.0004). Bottom: images of Pair1 GCaMP6f fluorescence pre- and post-Chrimson activation in ATR+ and ATR-
770 larvae. Genotype: *R49F02-Gal4^{AD} / R75C02-lexA; R53F07-Gal4^{DBD} / lexAop-GCaMP6f UAS-Chrimson:mCherry*.
771 (C) MDN and Pair 1 are co-active. Top: MDN and Pair1 expressing GCaMP6m in different regions of the neuropil, and
772 show concurrent activity. Bottom: MDNs (white arrowhead) and Pair1 (yellow arrowhead) show similar timing of
773 GCaMP6m fluorescence during a BWD wave. Anterior, up; midline, right side of panel. MDN and Pair1 co-activity
774 was observed in 5 out of 10 brains examined; the other 5 brains showed Pair1 activity but no MDN activity (see
775 Supplement to Figure 6). Genotype: *ss01613-Gal4 / UAS-GCaMP6m; R75C02-Gal4*.
776 (D) Pair1 is active during backward (BWD) but not forward (FWD) waves in fictive preparations. Left: Quantification
777 of Pair1 GCaMP6m activity (bottom) and motor neuron activity (top) during fictive BWD and FWD waves in the same
778 animal. Pair1 is not active during FWD waves. Right: Pair1 GCaMP6m activity (arrowheads) precedes U1-U5 motor
779 neuron activity (circled) and only occurs during BWD motor waves. N = 53 BWD waves from 7 different animals, and
780 14 FWD waves from 4 different animals. Genotype: *CQ-lexA / UAS-GCaMP6m; lexAop-GCaMP6m / R94E10-Gal4*.
781 (E) Pair1 is preferentially active during backward locomotion in the intact animal. CaMPARI was expressed in Pair1
782 and photoconversion was activated during FWD or BWD locomotion in intact third instar larvae. There is
783 significantly more CaMPARI photoconversion during BWD locomotion. Graph, quantification of red fluorescence
784 over green fluorescence mean intensity. Triangle or square, data from an individual axon. n= 36 for FWD and 34 for
785 BWD. Scale bar, 10 µm. Genotype: *R72C02-Gal4 UAS-CaMPARI.*
786
787

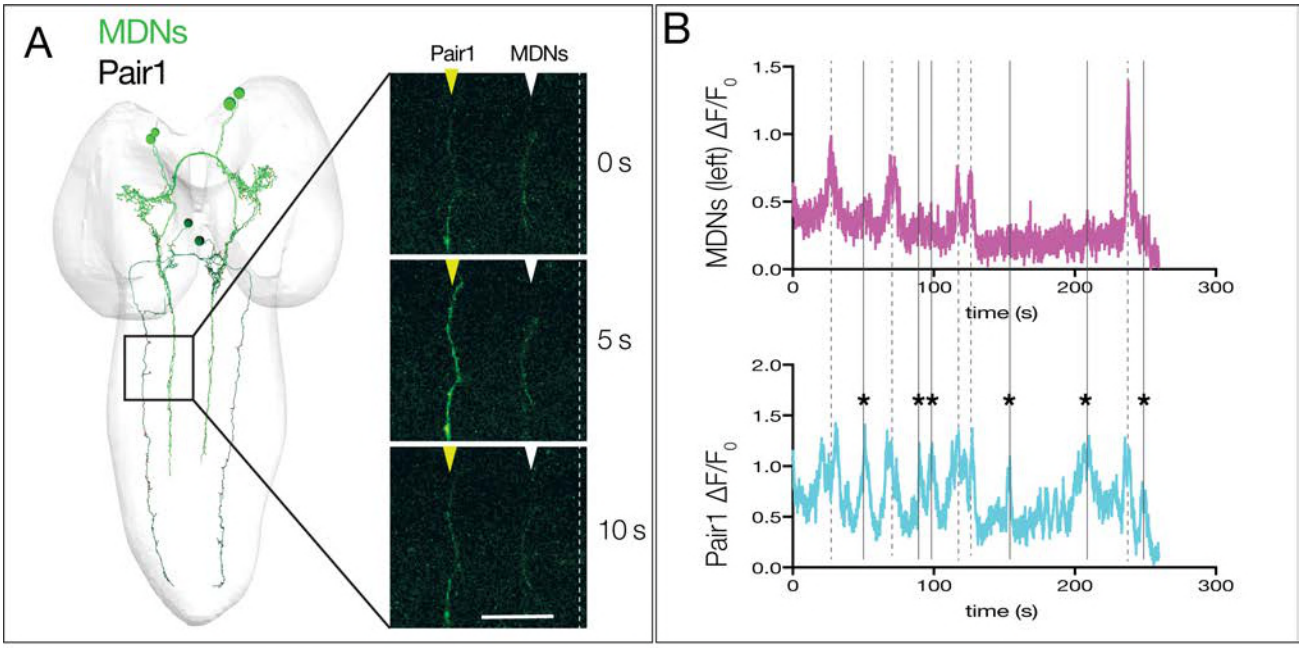

Supplement to Figure 6

Supplement to Figure 6. Pair1 can be activated independent of MDN activity.
(A) Left: dorsal view of TEM reconstruction of Pair1 and MDNs in a first instar larval CNS. Right: GCaMP6m activity in MDNs (white arrowheads) and Pair1 (yellow arrowheads) at three different time points in a third instar larval CNS fictive preparation. Pair1 is active while MDNs stay inactive. Anterior, up; midline, dashed line. Scale bar, 30 µm. (B,C) GCaMP6m activation in MDNs (top) and Pair1 (bottom) in a third instar larval CNS showing Pair1 activity concurrent with MDN activity (dashed lines) and Pair1 activity independent of MDN activity (solid lines, asterisk). Genotype: *ss01613-Gal4 / UAS-GCaMP6m; R75C02-Gal4*.

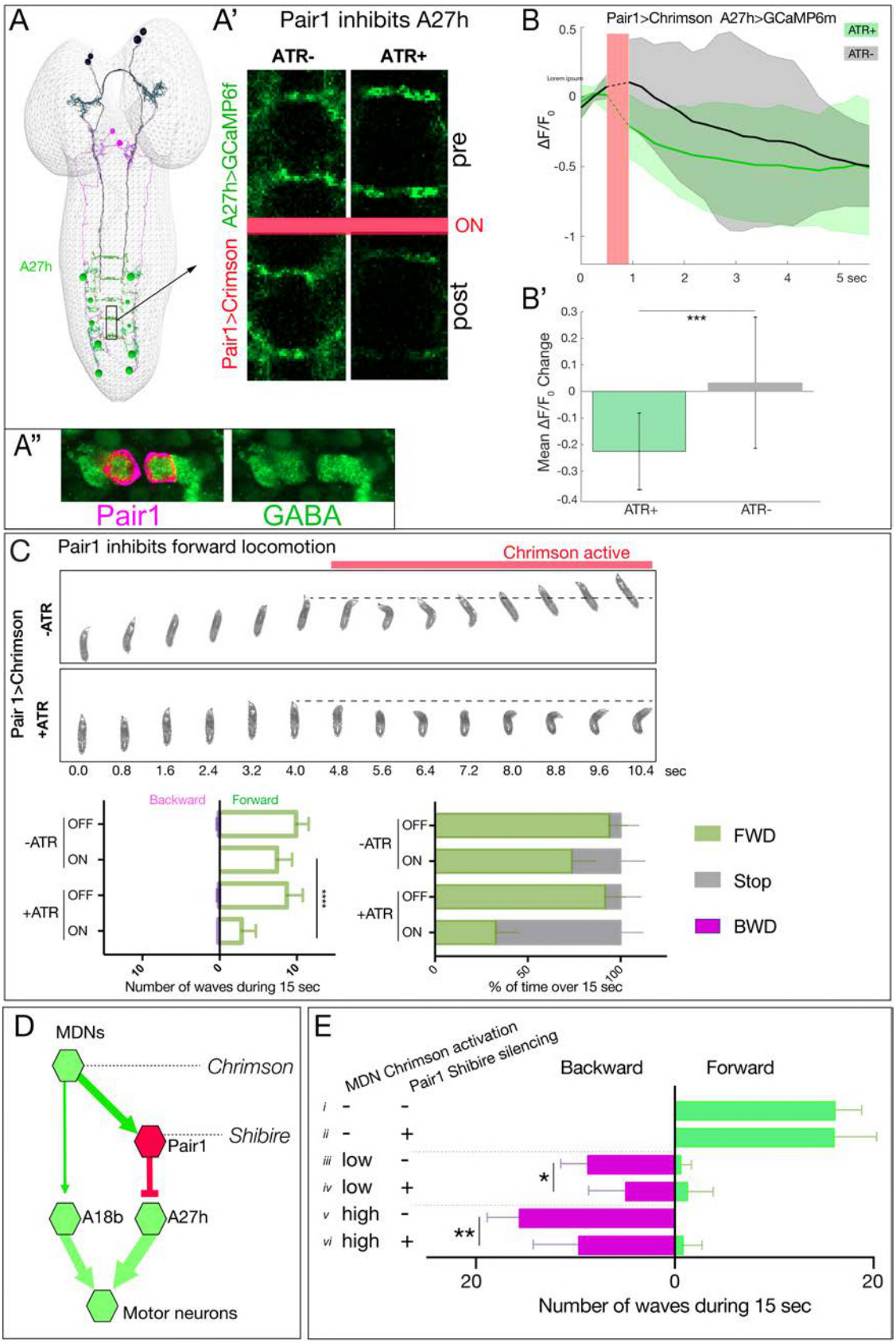

Figure 7

797

Figure 7. Pair1 inhibits the forward-active A27h premotor neuron, and arrests forward locomotion.

(A,B) Pair1 inhibits A27h. (A) Reconstruction of MDNs (black), Pair1 neurons (magenta) and A27h neurons (green) in the first instar CNS TEM volume. (A') A27h GCaMP6m fluorescence is reduced following Pair1 Chrimson activation (red bar); two segments shown. (A'') Pair1 is GABAergic. Pair1 cell body (mCherry; magenta, arrowheads) and GABA (green). Genotype: *R75C02-Gal4, UAS-Chrimson:mCherry.* (B) A27h GCaMP6m fluorescence is reduced following Pair1 Chrimson activation (red bar). (B') $\Delta F/F_0$ was significantly inhibited in ATR+ animals relative to ATR- controls. A total of 26 events from 7 animals were averaged for ATR+ and 16 events from 4 animals for ATR- group. See methods for further details. Genotype: *R75C02-lexA/+; lexAop-Chrimson:mCherry / R36G02-Gal4, UAS-GCaMP6m.*
(C) Activation of Pair1 halts FWD locomotion for the duration of neuronal activation. Top, time-lapse images of +/- ATR larvae expressing Chrimson in Pair1 neurons before and during light stimulation. Bottom left, backward and forward wave number over 15s without Chrimson activation (Off) or during Chrimson activation (On) in third instar larvae. n = 12 for all groups. Bottom right, percent time performing forward locomotion (green), backward locomotion (magenta) or not moving (grey) over 15s without Chrimson activation (Off) or during Chrimson activation (On) in third instar larvae. n = 5 for all groups. Genotype: *R72C02-Gal4 UAS-Chrimson:mVenus.*
(D) Schematic illustrating the experiment in (E). Arrows, excitatory connections; T-bar, inhibitory connection; line width proportional to synapse number.
(E) Pair1 activity is necessary for efficient Chrimson-induced backward locomotion. Chrimson was expressed in MDNs, and shibire^{ts} was expressed in Pair1 neurons. Low (0.07mW/mm^2) or high (0.275mW/mm^2) light intensities were used to induce MDN activity; a temperature shift to 32^{o}C was used to inactivate Shibire^{ts} and thus silence Pair1 neurons. Silencing of Pair1 alone had no detectable phenotype (i, ii). Silencing Pair1 decreased the efficacy of MDN-induced backward locomotion at low or high light levels (iii-vi). Genotypes: *R49F02-Gal4^{AD} R53F07-Gal4^{DBD} UAS-Chrimson:mVenus pBD-lexA lexAop-Shibire^{ts}* (*i*, *iii* and *v*) and *R49F02-Gal4^{AD} R53F07-Gal4^{DBD} UAS-Chrimson:mVenus 75C02-lexA lexAop-Shi^{ts1}* (*ii, iv* and *vi*).

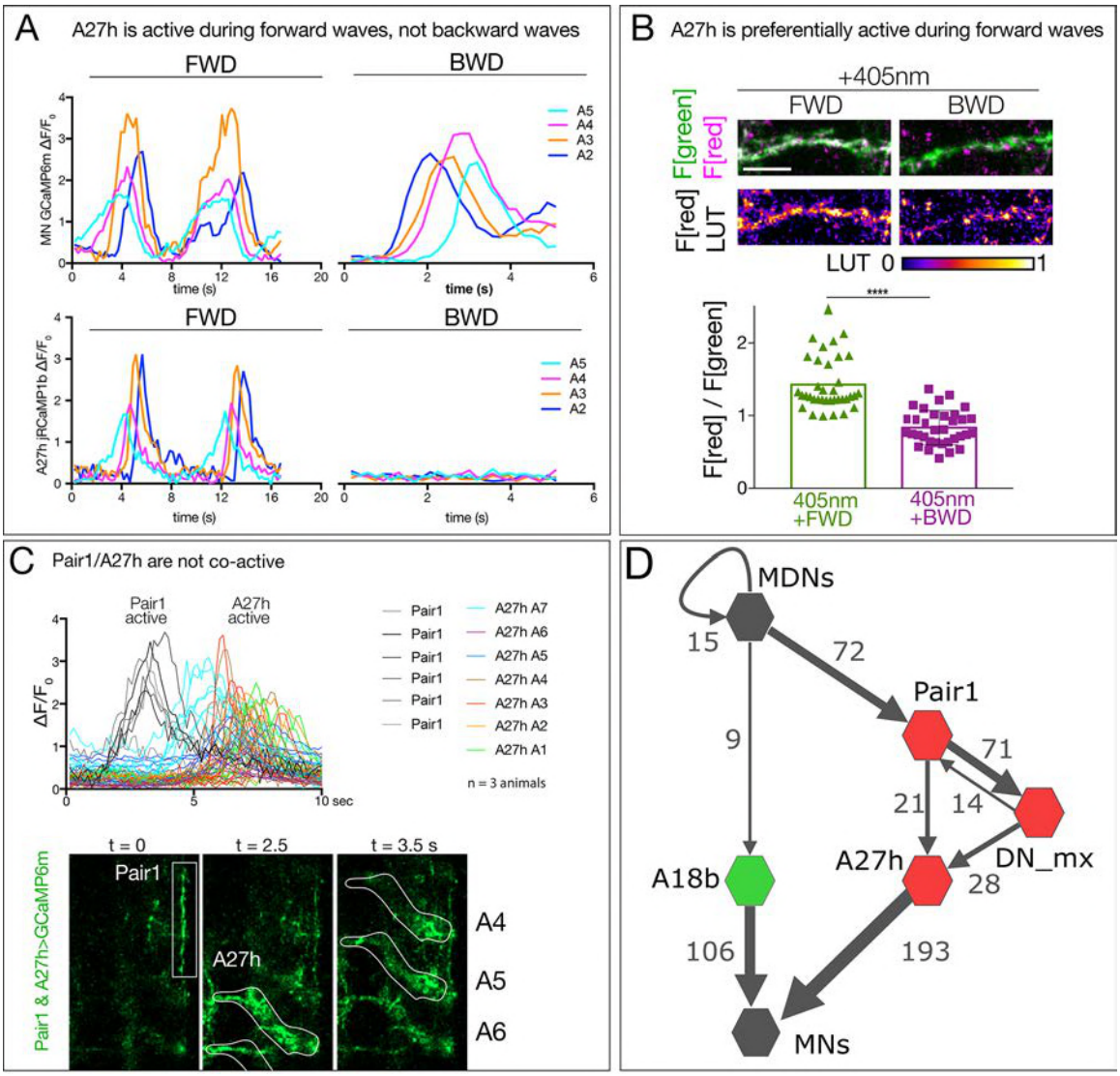

Supplement to Figure 7. Timing of A27h neuronal activity.

(A) A27h is active during forward (FWD) but not backward (BWD) motor waves in fictive preparations. A27h expresses jRCaMP1b and U1-U5 motor neurons express GCaMP6m. Genotype: *CQ-lexA/+ ; lexAop-GCaMP6m/R36G02-Gal4,UAS-jRCaMP1b*

(B) A27h is preferentially active during forward locomotion in the intact animal. CaMPARI in A27h neurites of a third instar larval CNS. Top, fluorescence emission following 488nm (green) or 561nm (red) illumination. Bottom, graph represents quantification of red fluorescence over green fluorescence mean intensity. Each value represents data from an individual axon. n= 17 for FWD and 16 for BWD. Scale bar, 10 µm. Genotype: *R36G02-Gal4 UAS-CaMPARI*.

(C) Pair1 and A27h are not co-active. GCaMP6m fluorescence was measured in distinct ROIs for Pair1 and A27h (bottom panels). Traces show six Pair1 neurons (gray lines) and 42 A27h neurons from segments A1-A7 from three animals (colored lines). Note that forward waves of A27h activity follow but don't overlap with the time of Pair1 activity. Genotype: *R75C02-Gal4/R36G02-Gal4, UAS-GCaMP6m.*

(D) There is no direct anatomical connection between A27h and A18b pathways. Neurons with one or more synapse in the TEM reconstruction are shown (numbers next to arrows).

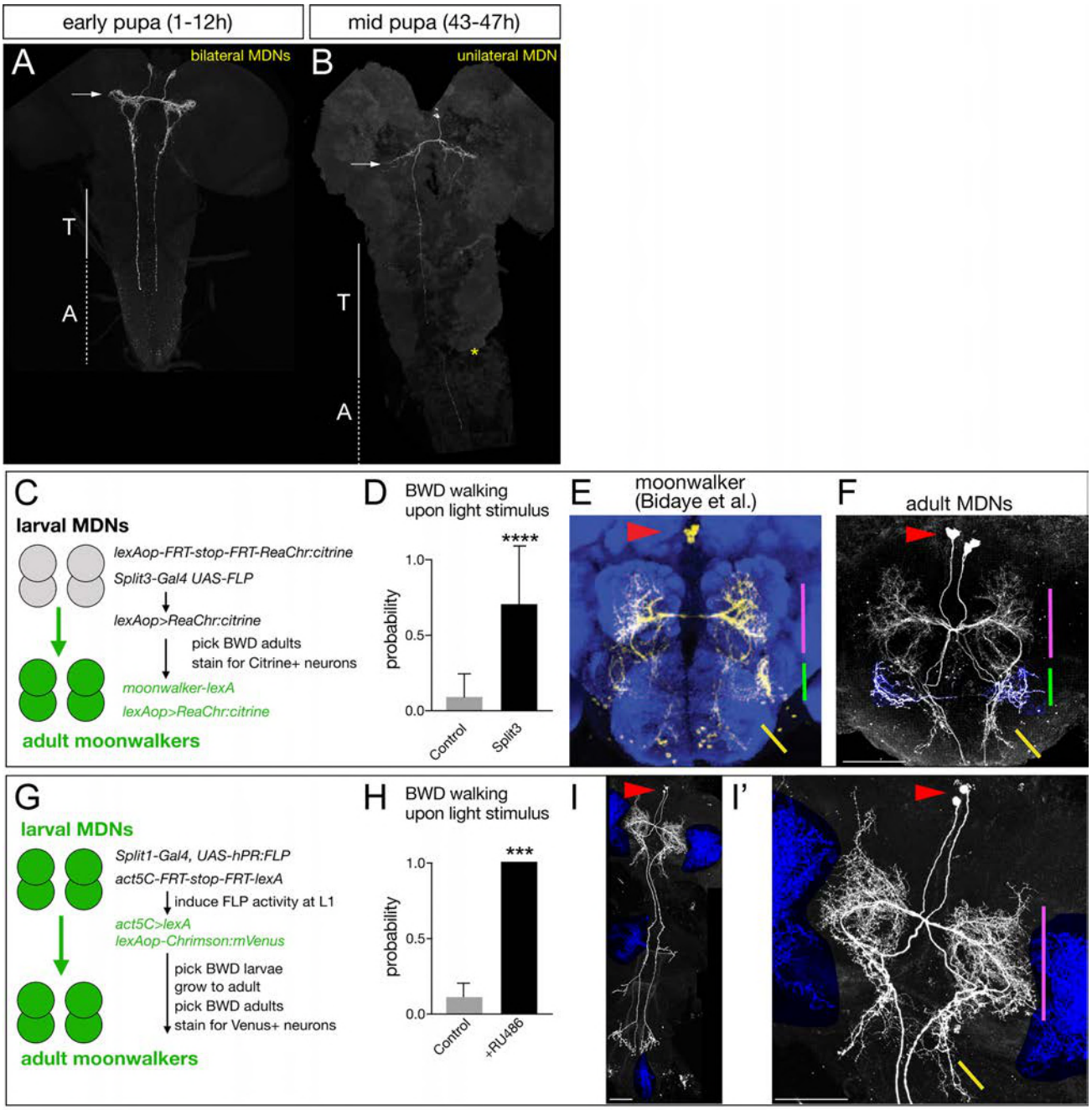

Figure 8

839

Figure 8. Larval MDNs persist into adulthood, match the moonwalker neuron morphology, and induce backward walking

(A-B) MDN neurons labeled by Split1 MCFO are similar in morphology to larval neurons during early pupal stages (A), but prune their brain and SEZ arbors by mid-pupal stages (B, arrow). T, thoracic segments; A, abdominal segments. Asterisk, tissue damage from dissection.

(C-F) Larval MDNs persist to adulthood, match adult moonwalker morphology, and can induce backward walking in adults. (C) Genetic scheme for the experiment. (D) Probability of adult backward walking upon light activation of Split3 immortalized neurons (split3) or controls lacking the DBD half of Split3 genotype (control). (E) Adult moonwalker neurons from Bidaye et al., 2014. Red arrowhead, cell bodies; colored lines, distinctive arbors. (F) One example of 'immortalized' larval MDNs showing the same cell body location (red arrowhead) and same distinctive arbors (colored lines); however, we find that the arbor marked by the green line is an off-target projection not connected to the MDN neurons. Genotypes: Control: *UAS-FLP.PEST ss01613-(AD)-Gal4/TM3 VT044845-lexA lexAop-FRT-stop-FRT-ReaChr:citrine*. Split3: *UAS-FLP.PEST ss01613-(AD+DBD)-Gal4 VT044845-lexA lexAop-FRT-stop-FRT-ReaChr:citrine*.

(G-I) Larval MDNs persist to adulthood and induce backward walking. (G) Intersectional genetics used in this experiment. (H) Probability of adult backward walking upon light activation of the neurons immortalized by RU486-induced Flp activity (RU486+) or controls not given RU486 and thus lacking Chrimson expression in adult MDNs (control). (I) One example of an adult CNS plus VNC showing two MDNs (arrowhead) and four off target neurons (blue shading). (I') Enlargement of brain showing MDNs and parts of two off target neurons (blue shading). Red arrowhead, cell bodies; colored lines, distinctive arbors in the protocerebrum (magenta line) and SEZ (green line).

Scale bars, 50 µm.

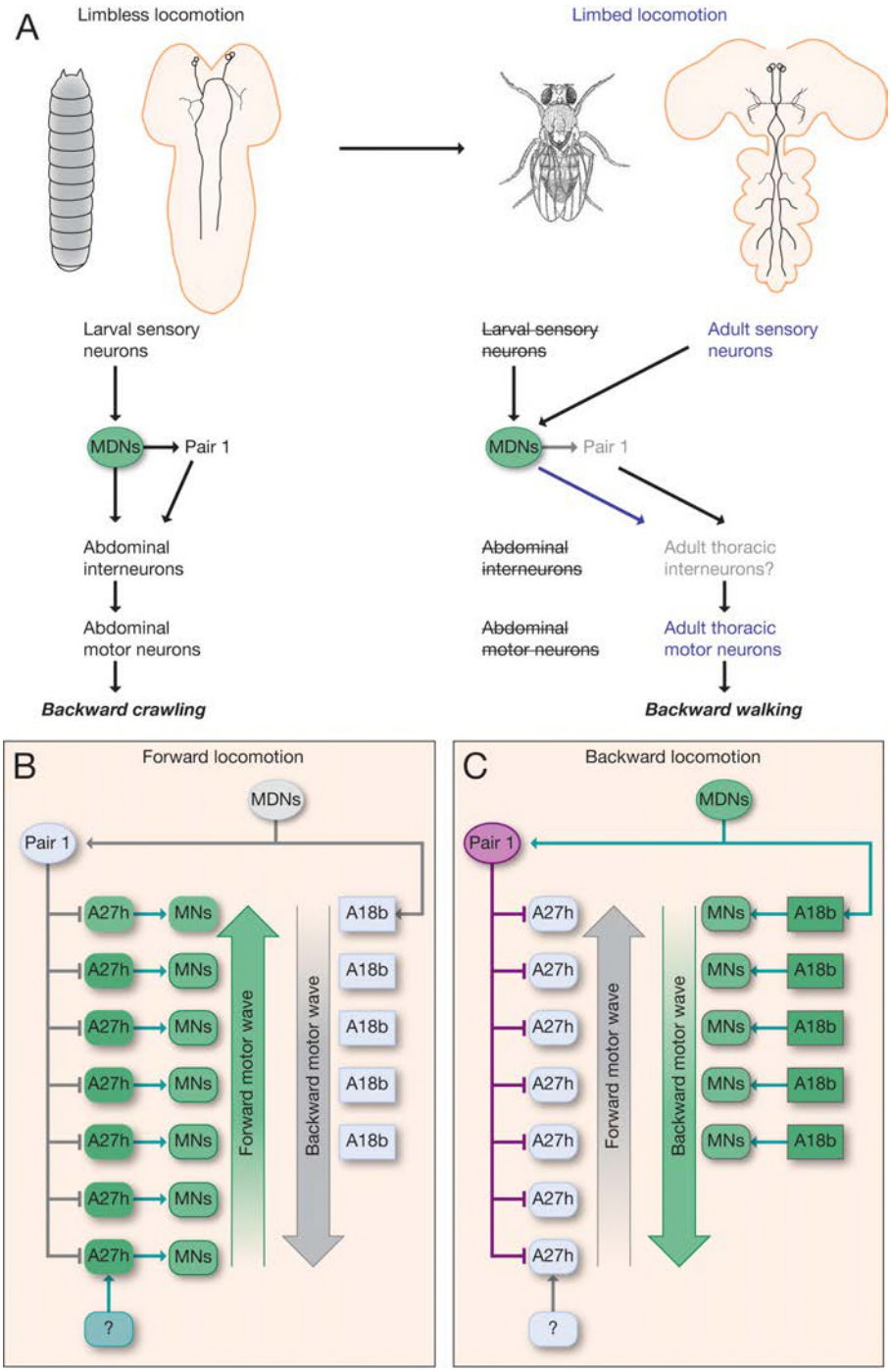

Figure 9. Model describing the MDN-mediated backward crawling.

(A) MDN neurons are present in larval stages where they promote backward peristaltic crawling via abdominal premotor and motor neurons; MDNs subsequently persist into the adult fly where they promote backward walking of the six-limbed adult fly, using a different pool of thoracic motor neurons.

(B,C) Model. (B) During forward locomotion the MDNs, Pair1 and A18b are silent; an unknown neuron (?) may initiate forward locomotion. (C) During backward locomotion the MDNs are activated which in turn activates Pair1 descending neuron. Pair1 activity inhibits the forward-active A27h premotor neuron to halt forward locomotion, and activates the backward-active A18b premotor neuron to initiate a backward motor wave.

872 **Movie 1a,b. MDN activation induces backward larval locomotion.**
873 Crawling behavior of third instar larvae expressing Chrimson in MDNs (Split1>Chrimson:mVenus) with ATR (a) or
874 without ATR (b). During the first 15 seconds, the animals are not under optogenetic light followed by 15 seconds
875 under 0.5 mW/mm^2 of green light.
876
877 **Movie 2a,b. Pair1 activation blocks forward locomotion.**
878 Crawling behavior of third instar larvae expressing Chrimson in Pair1 (75C02>Chrimson:mVenus) with ATR (a) or
879 without ATR (b). During the first 10 seconds, the animals are not under optogenetic light followed by 10 seconds
880 under 0.28 mW/mm^2 of green light.
881
882 **Movie 3. Larval MDNs persist into adulthood and induce backward walking.**
883 Walking behavior of adult flies carrying all the components showed in 8F (split3, right) or all the genetic components
884 except the DBD half of Split3 (control, left). During the first 10 seconds, the animals are not under optogenetic light
885 followed by 10 seconds under 0.28 mW/mm^2 of red light.
886
887 **Supplemental File 1. Graph view of the MDN and downstream neurons.**
888 File can be opened in CATMAID using the graph widget.
889

References

Bainbridge, S.P., and M. Bownes. 1981. Staging the metamorphosis of Drosophila melanogaster. *J Embryol Exp Morphol*. 66:57-80.

Berni, J. 2015. Genetic Dissection of a Regionally Differentiated Network for Exploratory Behavior in Drosophila Larvae. *Current biology : CB*. 25:1319-1326.

Berni, J., S.R. Pulver, L.C. Griffith, and M. Bate. 2012. Autonomous circuitry for substrate exploration in freely moving Drosophila larvae. *Current biology : CB*. 22:1861-1870.

Bidaye, S.S., C. Machacek, Y. Wu, and B.J. Dickson. 2014. Neuronal control of Drosophila walking direction. *Science (New York, N.Y.)*. 344:97-101.

Bouvier, J., V. Caggiano, R. Leiras, V. Caldeira, C. Bellardita, K. Balueva, A. Fuchs, and O. Kiehn. 2015. Descending Command Neurons in the Brainstem that Halt Locomotion. *Cell*. 163:1191-1203.

Clark, M.Q., S.J. McCumsey, S. Lopez-Darwin, E.S. Heckscher, and C.Q. Doe. 2016. Functional Genetic Screen to Identify Interneurons Governing Behaviorally Distinct Aspects of Drosophila Larval Motor Programs. *G3 (Bethesda)*. 6:2023-2031.

Clark, M.Q., A.A. Zarin, A. Carreira-Rosario, and C.Q. Doe. 2018. Neural circuits driving larval locomotion in Drosophila. *Neural development*. 13:6.

Dolan, M.-J., H. Luan, W.C. Shropshire, B. Sutcliffe, B. Cocanougher, R.L. Scott, S. Frechter, M. Zlatic, G.S.X.E. Jefferis, and B.H. White. 2017. Facilitating Neuron-Specific Genetic Manipulations in Drosophila melanogaster Using a Split GAL4 Repressor. *Genetics*. 206.

Dubuc, R., F. Brocard, M. Antri, K. Fenelon, J.F. Gariepy, R. Smetana, A. Menard, D. Le Ray, G. Viana Di Prisco, E. Pearlstein, M.G. Sirota, D. Derjean, M. St-Pierre, B. Zielinski, F. Auclair, and D. Veilleux. 2008. Initiation of locomotion in lampreys. *Brain Res Rev*. 57:172-182.

Fosque, B.F., Y. Sun, H. Dana, C.T. Yang, T. Ohyama, M.R. Tadross, R. Patel, M. Zlatic, D.S. Kim, M.B. Ahrens, V. Jayaraman, L.L. Looger, and E.R. Schreiter. 2015. Neural circuits. Labeling of active neural circuits in vivo with designed calcium integrators. *Science*. 347:755-760.

Fushiki, A., H. Kohsaka, and A. Nose. 2013. Role of sensory experience in functional development of Drosophila motor circuits. *PLoS One*. 8:e62199.

Fushiki, A., M.F. Zwart, H. Kohsaka, R.D. Fetter, A. Cardona, and A. Nose. 2016. A circuit mechanism for the propagation of waves of muscle contraction in Drosophila. *eLife*. 5.

Grillner, S., and A. El Manira. 2015. The intrinsic operation of the networks that make us locomote. *Curr Opin Neurobiol*. 31:244-249.

Hagglund, M., L. Borgius, K.J. Dougherty, and O. Kiehn. 2010. Activation of groups of excitatory neurons in the mammalian spinal cord or hindbrain evokes locomotion. *Nat Neurosci*. 13:246-252.

Hampel, S., R. Franconville, J.H. Simpson, and A.M. Seeds. 2015. A neural command circuit for grooming movement control. *The Journal of Neuroscience*. 4:8079-8091.

Harris, R.M., B.D. Pfeiffer, G.M. Rubin, and J.W. Truman. 2015. Neuron hemilineages provide the functional ground plan for the Drosophila ventral nervous system. *eLife*. 4.

Heckscher, E.S., S.R. Lockery, and C.Q. Doe. 2012. Characterization of Drosophila larval crawling at the level of organism, segment, and somatic body wall musculature. *The Journal of neuroscience : the official journal of the Society for Neuroscience*. 32:12460-12471.

Heckscher, E.S., A.A. Zarin, S. Faumont, M.Q. Clark, L. Manning, A. Fushiki, C.M. Schneider-Mizell, R.D. Fetter, J.W. Truman, M.F. Zwart, M. Landgraf, A. Cardona, S.R. Lockery, and

C.Q. Doe. 2015. Even-Skipped(+) Interneurons Are Core Components of a Sensorimotor Circuit that Maintains Left-Right Symmetric Muscle Contraction Amplitude. *Neuron*. 88:314-329.

Hedwig, B. 2000. Control of cricket stridulation by a command neuron: efficacy depends on the behavioral state. *Journal of neurophysiology*. 83:712-722.

Hückesfeld, S., A. Schoofs, P. Schlegel, A. Miroschnikow, and M.J. Pankratz. 2015. Localization of motor neurons and central pattern generators for motor patterns underlying feeding behavior in drosophila larvae. *PLoS ONE*. 10.

Hughes, C.L., and J.B. Thomas. 2007. A sensory feedback circuit coordinates muscle activity in Drosophila. *Mol Cell Neurosci*. 35:383-396.

Jordan, L.M., J. Liu, P.B. Hedlund, T. Akay, and K.G. Pearson. 2008. Descending command systems for the initiation of locomotion in mammals. *Brain Research Reviews*. 57:183-191.

Juvin, L., S. Gratsch, E. Trillaud-Doppia, J.F. Gariepy, A. Buschges, and R. Dubuc. 2016. A Specific Population of Reticulospinal Neurons Controls the Termination of Locomotion. *Cell Rep*. 15:2377-2386.

Kallman, B.R., H. Kim, and K. Scott. 2015. Excitation and inhibition onto central courtship neurons biases Drosophila mate choice. *eLife*. 4:e11188.

Kendroud, S., A.A. Bohra, P.A. Kuert, B. Nguyen, O. Guillermin, S.G. Sprecher, H. Reichert, K. VijayRaghavan, and V. Hartenstein. 2018. Structure and development of the subesophageal zone of the Drosophila brain. II. Sensory compartments. *The Journal of comparative neurology*. 526:33-58.

Kernan, M., D. Cowan, and C. Zuker. 1994. Genetic dissection of mechanosensory transduction: mechanoreception-defective mutations of Drosophila. *Neuron*. 12:1195-1206.

Kernan, M.J. 2007. Mechanotransduction and auditory transduction in Drosophila. *Pflugers Arch*. 454:703-720.

Kimura, Y., C. Satou, S. Fujioka, W. Shoji, K. Umeda, T. Ishizuka, H. Yawo, and S. Higashijima. 2013. Hindbrain V2a neurons in the excitation of spinal locomotor circuits during zebrafish swimming. *Curr Biol*. 23:843-849.

King, D.G., and R.J. Wyman. 1980. Anatomy of the giant fibre pathway in Drosophila. I. Three thoracic components of the pathway. *J Neurocytol*. 9:753-770.

Koyama, M., F. Minale, J. Shum, N. Nishimura, C.B. Schaffer, and J.R. Fetcho. 2016. A circuit motif in the zebrafish hindbrain for a two alternative behavioral choice to turn left or right. *eLife*. 5.

Kristan, W.B. 2008. Neuronal decision-making circuits. *Current biology : CB*. 18:R928-932.

Landgraf, M., V. Jeffrey, M. Fujioka, J.B. Jaynes, and M. Bate. 2003. Embryonic origins of a motor system: motor dendrites form a myotopic map in Drosophila. *PLoS Biol*. 1:E41.

Landgraf, M., and S. Thor. 2006. Development of Drosophila motoneurons: Specification and morphology. *Seminars in Cell & Developmental Biology*. 17:3-11.

Lindsay, T.H., T.R. Thiele, and S.R. Lockery. 2011. Optogenetic analysis of synaptic transmission in the central nervous system of the nematode Caenorhabditis elegans. *Nature communications*. 2:306.

Liu, K.S., and J.R. Fetcho. 1999. Laser ablations reveal functional relationships of segmental hindbrain neurons in zebrafish. *Neuron*. 23:325-335.

Luan, H., N.C. Peabody, C.R. Vinson, and B.H. White. 2006. Refined spatial manipulation of neuronal function by combinatorial restriction of transgene expression. *Neuron*. 52:425-436.

Medan, V., and T. Preuss. 2014. The Mauthner-cell circuit of fish as a model system for startle plasticity. *J Physiol Paris*. 108:129-140.

Mohammad, F., J.C. Stewart, S. Ott, K. Chlebikova, J.Y. Chua, T.-W. Koh, J. Ho, and A. Claridge-Chang. 2017. Optogenetic inhibition of behavior with anion channelrhodopsins. *Nature Methods*. 14.

Nern, A., B.D. Pfeiffer, and G.M. Rubin. 2015. Optimized tools for multicolor stochastic labeling reveal diverse stereotyped cell arrangements in the fly visual system. *Proceedings of the National Academy of Sciences of the United States of America*. 112:E2967-2976.

Ohyama, T., C.M. Schneider-Mizell, R.D. Fetter, J.V. Aleman, R. Franconville, M. Rivera-Alba, B.D. Mensh, K.M. Branson, J.H. Simpson, J.W. Truman, A. Cardona, and M. Zlatic. 2015. A multilevel multimodal circuit enhances action selection in Drosophila. *Nature*. 520:633-639.

Pearson, K.G., D.N. Reye, D.W. Parsons, and G. Bicker. 1985. Flight-initiating interneurons in the locust. *Journal of neurophysiology*. 53:910-925.

Pfeiffer, B.D., A. Jenett, A.S. Hammonds, T.-T.B. Ngo, S. Misra, C. Murphy, A. Scully, J.W. Carlson, K.H. Wan, T.R. Laverty, C. Mungall, R. Svirskas, J.T. Kadonaga, C.Q. Doe, M.B. Eisen, S.E. Celniker, and G.M. Rubin. 2008. Tools for neuroanatomy and neurogenetics in Drosophila. *Proceedings of the National Academy of Sciences of the United States of America*. 105:9715-9720.

Piggott, B.J., J. Liu, Z. Feng, S.A. Wescott, and X.Z. Xu. 2011. The neural circuits and synaptic mechanisms underlying motor initiation in C. elegans. *Cell*. 147:922-933.

Pulver, S.R., T.G. Bayley, A.L. Taylor, J. Berni, M. Bate, and B. Hedwig. 2015. Imaging fictive locomotor patterns in larval Drosophila. *Journal of neurophysiology*. 114:2564-2577.

Rickert, C., T. Kunz, K.-L. Harris, P.M. Whitington, and G.M. Technau. 2011. Morphological characterization of the entire interneuron population reveals principles of neuromere organization in the ventral nerve cord of Drosophila. *The Journal of neuroscience : the official journal of the Society for Neuroscience*. 31:15870-15883.

Roberts, A., W.C. Li, S.R. Soffe, and E. Wolf. 2008. Origin of excitatory drive to a spinal locomotor network. *Brain Res Rev*. 57:22-28.

Roberts, W.M., S.B. Augustine, K.J. Lawton, T.H. Lindsay, T.R. Thiele, E.J. Izquierdo, S. Faumont, R.A. Lindsay, M.C. Britton, N. Pokala, C.I. Bargmann, and S.R. Lockery. 2016. A stochastic neuronal model predicts random search behaviors at multiple spatial scales in C. elegans. *eLife*. 5.

Robertson, J.L., A. Tsubouchi, and W.D. Tracey. 2013. Larval Defense against Attack from Parasitoid Wasps Requires Nociceptive Neurons. *PLOS ONE*. 8:e78704.

Schneider-Mizell, C.M., S. Gerhard, M. Longair, T. Kazimiers, F. Li, M.F. Zwart, A. Champion, F.M. Midgley, R.D. Fetter, S. Saalfeld, and A. Cardona. 2016. Quantitative neuroanatomy for connectomics in Drosophila. *eLife*. 5.

Sen, R., M. Wu, K. Branson, A. Robie, G.M. Rubin, and B.J. Dickson. 2017. Moonwalker Descending Neurons Mediate Visually Evoked Retreat in Drosophila. *Current Biology*. 27:766-771.

Takagi, S., B.T. Cocanougher, S. Niki, D. Miyamoto, H. Kohsaka, H. Kazama, R.D. Fetter, J.W. Truman, M. Zlatic, A. Cardona, and A. Nose. 2017. Divergent Connectivity of Homologous Command-like Neurons Mediates Segment-Specific Touch Responses in Drosophila. *Neuron*. 96:1373-1387.e1376.

Tanouye, M.A., and R.J. Wyman. 1980. Motor outputs of giant nerve fiber in Drosophila. *Journal of neurophysiology*. 44:405-421.

Titlow, J.S., J. Rice, Z.R. Majeed, E. Holsopple, S. Biecker, and R.L. Cooper. 2014. Anatomical and genotype-specific mechanosensory responses in Drosophila melanogaster larvae. *Neuroscience research*. 83:54-63.

Tracey, W.D., Jr., R.I. Wilson, G. Laurent, and S. Benzer. 2003. painless, a Drosophila gene essential for nociception. *Cell*. 113:261-273.

Vogelstein, J.T., Y. Park, T. Ohyama, R.A. Kerr, J.W. Truman, C.E. Priebe, and M. Zlatic. 2014. Discovery of Brainwide Neural-Behavioral Maps via Multiscale Unsupervised Structure Learning. *Science*. 344:386-392.

von Philipsborn, A.C., T. Liu, J.Y. Yu, C. Masser, S.S. Bidaye, and B.J. Dickson. 2011. Neuronal control of Drosophila courtship song. *Neuron*. 69:509-522.

Weber, F., S. Chung, K.T. Beier, M. Xu, L. Luo, and Y. Dan. 2015. Control of REM sleep by ventral medulla GABAergic neurons. *Nature*. 526:435-438.

Wu, C.L., T.F. Fu, Y.Y. Chou, and S.R. Yeh. 2015. A single pair of neurons modulates egg-laying decisions in Drosophila. *PLoS One*. 10:e0121335.

Zwart, M.F., S.R. Pulver, J.W. Truman, A. Fushiki, R.D. Fetter, A. Cardona, and M. Landgraf. 2016. Selective Inhibition Mediates the Sequential Recruitment of Motor Pools. *Neuron*. 91:615-628.